PROBABILISTIC SLOPE STABILITY ASSESSMENT OF SUBMARINE LANDSLIDES BY THE USE OF BAYESIAN INFERENCE

A Thesis

by

RONEET DAS

Submitted to the Office of Graduate and Professional Studies of
Texas A&M University
in partial fulfillment of the requirements for the degree of

MASTER OF SCIENCE

Chair of Committee,	Zenon Medina-Cetina
Co-Chair of Committee,	Charles Aubeny
Committee Member,	Jihoon Kim
Head of Department,	Robin Autenrieth

May 2016

Major Subject: Civil Engineering

ABSTRACT

Estimates of probability of slope failure based on Monte-Carlo methods depend upon the state of evidence on the slope stability model parameters. The Bayesian framework illustrated in this paper to estimate the probability of failure against submarine landslide incorporates experimental data (undrained shear strength) with the initial state of evidence on the model parameters to achieve more certain and accurate model predictions and estimates of probability of failure.

The objective of this research was to determine the probability of failure of a submarine slope due to static loading conditions for a given state of evidence (e.g. soil data, slope stability model and expert beliefs). A physics-based forward model (infinite slope) was adopted to evaluate the probability of failure against sliding. The geotechnical and geometric parameters (unit weight of the slice, thickness, pseudo-static seismic coefficient and slope angle) of the proposed model were regarded as random variables. The initial state of evidence and level of uncertainty associated with the proposed model parameters were presented as prior probability distribution functions (log-normal distribution). The Bayesian framework was adopted to calibrate the proposed model with synthetically generated experimental observations representing different in-situ undrained shear strength conditions.

Model predictions on the mobilized shear strength when sampled from posterior distributions of the model parameters showed greater certainty and accuracy with respect to the Monte-Carlo forward model simulations based on the prior distributions. Results

showed significant changes in the landslide probability with the increase in amount of data for two scenarios used for model calibration, while indicating the correlation structure changes among the model parameters. This allowed to estimating the sampling scenarios and their corresponding confidence gains prior to a field investigation.

ACKNOWLEDGEMENTS

I would like to thank my committee chair, Dr. Zenon Medina-Cetina, and my committee members, Dr. Charles Aubeny and Dr. Jihoon Kim, for their guidance and support throughout the course of this research.

Thanks also go to my friends and colleagues and the department faculty and staff for making my time at Texas A&M University a great experience. I also want to extend my gratitude to Jakin Chow for his initial contributions to this research.

Finally, thanks to my family for their encouragement and support throughout the course of my graduate program at Texas A&M University and my life.

TABLE OF CONTENTS

LIST OF FIGURES

Page

Page

LIST OF TABLES

Page

1. INTRODUCTION

Research by Pinder (2001) suggested that 14 billion tons of oil equivalent (btoe) of offshore oil reserves have been proved globally and more than 90% of the world's undiscovered hydrocarbon reserves lie offshore. King et al. (2011) suggested that arctic offshore regions and other offshore ice-frequented regions held a significant portion of the world's petroleum reserves. Therefore to produce from such offshore reserves, development of safe and reliable infrastructure such as subsea pipelines for production and transportation of crude oil or natural gas becomes necessary. Pipeline route selection is a vital component of pipeline engineering for safe and efficient transport of crude oil both onshore and offshore. According to Haneberg et al. (2013), "The route assessment process incorporates information about the locations of the pipeline termini, the material characteristics of the pipe and the fluid being transported, soil-pipe interaction, spanning potential, cultural features such as shipwrecks, actual and potential geohazard in the route." (para. 2).

Also, Bruschi et al. (2006), Morgenstern (1967), Randolph et al. (2012) and Zakeri et al. (2008) discuss the effect of turbidity currents and debris flow associated with submarine landslides on pipeline failure. They note that these are caused by earthquakes, collapsing slopes, and other geological disturbances. All of these factors can affect pipeline failure due to impact load and erosion of seabed leading to underwater canyons.

A number of geomechanical problems including avalanches, landslides, rock compression damages, offshore site investigation have been addressed using probabilistic methods such as the Bayesian inference. (Arson & Medina-Cetina 2015; Medina-Cetina et al. 2013; Medina-Cetina & Cepeda 2010; Ranali et al. 2010; Gauer et al. 2009). Qualitative and quantitative methods of slope stability analysis have been employed to assess the risk caused by landslides. Chowdhury and Flentje (2003) categorized risk as “very high” ,”high” ,”medium” ,”low” and “very low”. based on visual interpretation of bathymetry maps, which shows to be a useful way to conduct a qualitative assessment of the potential of landslides. Haneberg (2012) suggests that subsea slope stability could be assessed qualitatively based on the presence or absence of past landslides.

Quantitative risk assessment is increasingly gaining prevalence for slope stability analysis due to increasing computational power. Work by Haneberg (2004 & 2012), Haneberg et al. (2013), Ochoa et al. (2015), Remendo et al. (2008), Souza et al. (2014) and Wang et al. (2010), discuss quantitative methods for landslide risk assessment. Probabilistic methods such as FORM (First Order Reliabity Method), FOSM (First Order Second Moment) and Monte-Carlo simulations based on physical model for assessment of slope failures have been discussed and compared extensively by El-Ramly et al. (2002), Griffiths et al. (2009) and (2011). The effects of spatial variability of soil parameters, drainage conditions, and seismicity on the risk of landslide have been discussed in a probabilistic framework in Sivakumar and Mukesh (2003) and Griffiths et al. (2009). Griffiths and Fenton (2004) investigated the probability of failure of cohesive

slopes using an advanced probabilistic method called the random finite-element method (RFEM), which combines non-linear finite elements with random field generation techniques (Gordon & Vanmarcke 1990). Griffiths et al. (2009) demonstrates the disadvantages of a simplified probabilistic analyses which does not account for the spatial variability of soil properties as it leads to more non-conservative estimates of the probability of failure if the coefficient of variation of the shear strength parameters exceeds a critical value. Works by Lacasse and Nadim (2007) and Gilbert et al. (2014) indicate the importance of probabilistic geotechnical risk and reliability assessment for offshore applications while taking into account uncertainty associated with geotechnical properties and models.

Previous studies on quantitative risk assessment have not used the Bayesian framework on slope stability models to estimate probabilities of failure. Moreover, the impact of greater evidence on the model parameters (soil data, bathymetry data, etc.) and higher amount of experimental data on the model predictions, have not been studied on slope stability analysis. This paper uses the Bayesian framework to estimate the probabilities of failure against sliding, and studies the changes in these estimates with increasing amount of experimental data on the in-situ shear strength. As a first approach to illustrate the applicability of the Bayesian paradigm, a physics-based infinite slope model is introduced. The geotechnical and geometric model parameters such as unit weight of the slice, thickness, pseudo-static seismic coefficient and slope angle are defined here as random variables. Bayesian inference is adopted to obtain the full probabilistic description of the model parameters via a joint probability density function

called posterior. It facilitates the integration of the initial state of evidence about the model parameters and the observational data (in-situ undrained shear strength). The three basic components of the Bayesian framework are the prior distribution, likelihood function and the posterior distribution. The Bayesian paradigm allows the update of prior information about the model parameters conditioned on observational data. A major advantage of the Bayesian approach is its ability to reflect the state of confidence on the assessment of model parameters, conditioned on varying states of evidence (e.g. experimental observations, model complexity, and expert's beliefs).

The hypothesis of this work is to prove the influence of field sampling on the estimate of a slope's probability of failure a-priori.

The objectives of this work are:

1. To apply the Bayesian framework to the infinite slope model to estimate the probability of failure against sliding.
2. To achieve more certain and accurate model predictions of the mobilized shear strength.
3. To evaluate the impact of greater state of evidence of slope parameter on the estimation of the probability of failure.

2. METHODOLOGY

2.1 Limit Equilibrium Methods for Slope Stability Analysis

Methods using the limit equilibrium principle are some of the most common methods for analyzing slope stability. In these methods the factor of safety is derived from the conditions of equilibrium with respect to forces and moments. The mass of the soil in this case is discretized into elements, the free body diagram is drawn for each element, and the fundamental and constitutive equations are formulated at the element level. Some of the methods using limit equilibrium principles are the Fellenius Methods of Slices, Simplified Bishop Method, Corps of Engineers methods. Fredlund et al. (1981) describe a relationship between these methods, and suggests that the factor of safety equations for either circular or non-circular slip surface can be written in the same form only if force or moment equilibrium conditions are explicitly satisfied. The Limit Equilibrium Method is used on the infinite slope model.

2.2 Infinite Slope Model

The infinite slope idealization is the simplest model to conduct slope stability analysis. The approach consists in assuming an infinite slope of a given depth, with known soil unit weight and undrained shear strength parameters, and to consider the influence of earthquake by the use of a pseudo-seismic coefficient (that is, the earthquake movement is represented by a horizontal static force).

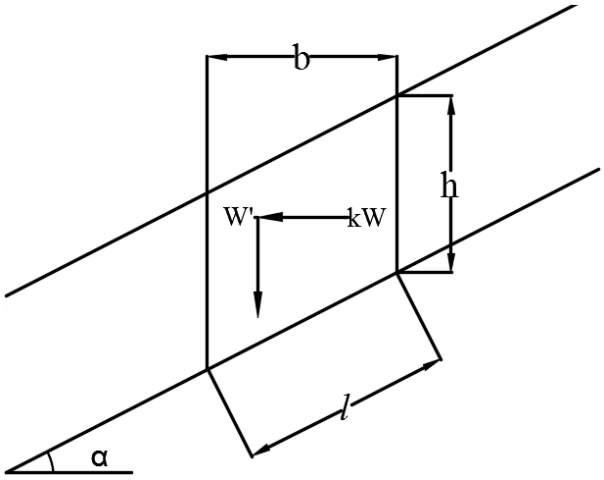

Fig. 2.1. Infinite slope model. (Morgenstern 1967)

Figure 2.1 represents the forces acting on a slice of an infinite slope. The plane of failure at a depth of 'h' is assumed to be at an angle 'α' with the horizontal. The equilibrium condition against sliding along the potential plane of failure is achieved when,

$$Resistance\ force = Loading\ force$$

The Resisting Force along the potential failure plane is the product of the undrained shear strength mobilized at the failure and a unit length along the base of the slice. The loading force is the summation of the component of the weight of the slice and the force due to earthquake effect parallel to the potential failure plane.

Considering the equilibrium of the slice shown the following equation can be formulated (Morgenstern 1967):

$$S_u \cdot l = W' sin\alpha + kW cos\alpha$$

Where,

S_u – Undrained shear strength developed along the potential slip surface

W' – submerged or buoyant weight of the slice, is defined as equal to $W'=\gamma' bh$

W – bulk/saturated weight of the slice, is defined as $W=\gamma bh$

l – length along the base of the slice, is defined as $l = b/\cos\alpha$

k – pseudo-static seismic coefficient (some percentage of the gravity)

α – slope angle

Substitute l, W' and W

$$S_u \cdot \left(\frac{b}{\cos\alpha}\right) = (\gamma' bh)\sin\alpha + k(\gamma bh)\cos\alpha$$

After rearrangement, the undrained shear strength S_u is equal to:

$$S_u = \gamma' h\left(\sin\alpha\cos\alpha + k\frac{\gamma}{\gamma'}\cos^2\alpha\right)$$

γ – saturated/bulks unit weight of the slice

γ' – buoyant/submerged unit weight of the slice

h – thickness of sediment above the slip surface

k – pseudo-static seismic coefficient (some percentage of the gravity)

α – slope angle

From the definitions of Resisting and Loading forces, it is then possible to define different safety criteria:

$$Factor\ of\ Safety = \frac{available\ shear\ strength}{mobilized\ shear\ strength}$$

$$= \frac{Resisting\ Force}{Loading\ Force}$$

$$FS = \frac{S_u}{\gamma' h(\sin\alpha\cos\alpha + k\frac{\gamma}{\gamma'}\cos^2\alpha)}$$

$$Safety\ Margin = Resistance\ force - Loading\ force$$

$$Probability\ of\ failure = \mathrm{P}(Safety\ Margin < 1)$$

$$Reliability = 1 - Probability\ of\ failure$$

2.3 Bayesian Framework

The Bayesian framework incorporates experimental data into initial state of evidence to achieve an updated state of evidence on the model parameters. The prior state of evidence on each model parameter is represented with a probability distribution function. The Bayesian framework to obtain the posterior probability distribution (probability distribution of the model parameters conditioned on observed data) can be established through the following form:

$$\pi(\theta|\mathrm{d}_{obs}) = \frac{f(\mathrm{d}_{obs}|\theta)\pi(\theta)}{\int f(\mathrm{d}_{obs}|\theta)\pi(\theta)d\theta}$$

Where,

$\pi(\theta)$ is the prior distribution

$f(\mathrm{d}_{obs}|\theta)$ is the likelihood function.

$\pi(\theta|\mathrm{d}_{obs})$ is the posterior distribution.

The posterior distribution of the parameters is also known as the target distribution from which random samples are taken. Sequences or chains of 600000 posterior values of model parameters were generated using the Markov Chain Monte-Carlo algorithm. Metropolis algorithm was used to accept or reject proposed values. The

posterior values of all the parameters attained a steady state distribution after 200000 iterations. Hence the burn-in point was set at 200000 and values from 200001 to 600000 were used for Monte-Carlo simulation of the forward model. Forward modeling of the infinite slope model sampled from the posterior values of the parameters show greater certainty and accuracy in the model parameters

3. CASE STUDY

A deep sea environment with stiff soil and high seismicity was considered for the research. A saturated unit weight ranging about 18-22 kN/m^3 and a pseudo-static seismic coefficient of about 0.2 characterized the geographical area under study. Infinite slope model is used to perform slope stability analysis for a representative area.

3.1. Infinite Slope Model Parameters

3.1.1. Soil Unit Weight (γ_{sat})

Saturated unit weight of the soil is determined from the sedimentology of the project area, the range of values for each type can be found to be from 12 kN/m^3 to 24 kN/m^3, (density kg/m^3 of 1.4-2.4) in previous works. Wang and Huang (2013) suggested that the unit weight follows a log normal distribution whereas (Haneberg 2004 & 2012) suggested that the unit weight can be presented as a truncated normal distribution.

3.1.2. Slope Angle (α)

The range of values of slope angles is obtained from the seabed bathymetry. Larger slope angles are a trigger to submarine landslides. (Locat & Lee 2000). However, studies presented in Prior and Coleman (1978) on the Mississippi delta (east Bay, Garden Island Bay, and shallow water areas adjacent to Pass a Loutre) suggest retrogressive landslides on slope angles as low as 0.01° to 0.45°.

3.1.3. Pseudo Static Seismic Coefficient (*k*)

The influence of an earthquake can be incorporated into the physics-based infinite slope model by introducing a horizontal body force, which is a fraction 'k' of the gravity. (Morgenstern 1967). Horizontal and vertical pseudostatic seismic coefficients k_h and k_v, respectively, are used to compute the horizontal and vertical forces caused by a potential earthquake on the slope. For simplicity of the model only the pseudo-horizontal static force of the earthquake is considered, therefore *k* in this case represents the *horizontal pseudo-static seismic coefficient, k_h*. Melo and Sharma (2004), suggest the value of k_h to about 0.4 to 0.45 times the peak horizontal acceleration. Usually assumed as the trigger and treated as a constant, say k=0.1, k=0.2.

3.1.4. Depth of Failure Plane (*h*)

Haneberg (2012) and (2004) assumed normal distribution Center at 5m and 4.42m respectively. Wang and Huang (2013) proposed the slice thickness following a lognormal distribution with mean 5m. Case studies however shown failure that could occur with height as high as 560 meters.

3.2. Prior Distributions of the Model Parameters

A probability distribution was assigned to each of the model parameters which represents the initial state of evidence and uncertainty associated with them. These distributions summarize the range of values that each of the model parameters may attain and hence are called the prior distributions. The distributions are often based upon expert opinion, historical data, experimental data on the parameters, etc. Random samples are drawn from these distributions to run Monte-Carlo simulation of the forward model,

which in this case is the infinite slope model. The model parameters are assumed to be independent of each other. $\pi(\theta)$ is the prior in the Bayesian framework and is the product of the individual priors of all the model parameters.

$$\pi(\theta) = \pi(\theta_1)* \pi(\theta_2)\ldots* \pi(\theta_n)$$

$$\pi(\theta) = \Pi\, \pi(\theta_n)$$

'n' represents the number of model parameters.

Table 3.1 presents the type, mean and standard deviation of the prior distributions of the model parameters. The values the model parameters could take were positive real numbers, hence log normal distributions were used for the prior distributions.

Parameter	Distribution	Mean	Standard Deviation
Saturated Unit Weight	Log-Normal	20 kN/m^3	3 kN/m^3
Depth of Failure Plane	Log-Normal	10 m	3 m
Slope Angle	Log-Normal	5°	1°
Pseudo-Static Seismic Coefficient	Log-Normal	0.2	0.05

Table 3.1. Prior probability distributions which represent the initial state of evidence on the model parameters.

Parameter	Distribution	Mean	Standard Deviation
Factor of Safety	Log-Normal	3	1

Table 3.1. Continued.

The graphical representation of the prior distributions of the model parameters is illustrated in figure 3.1.

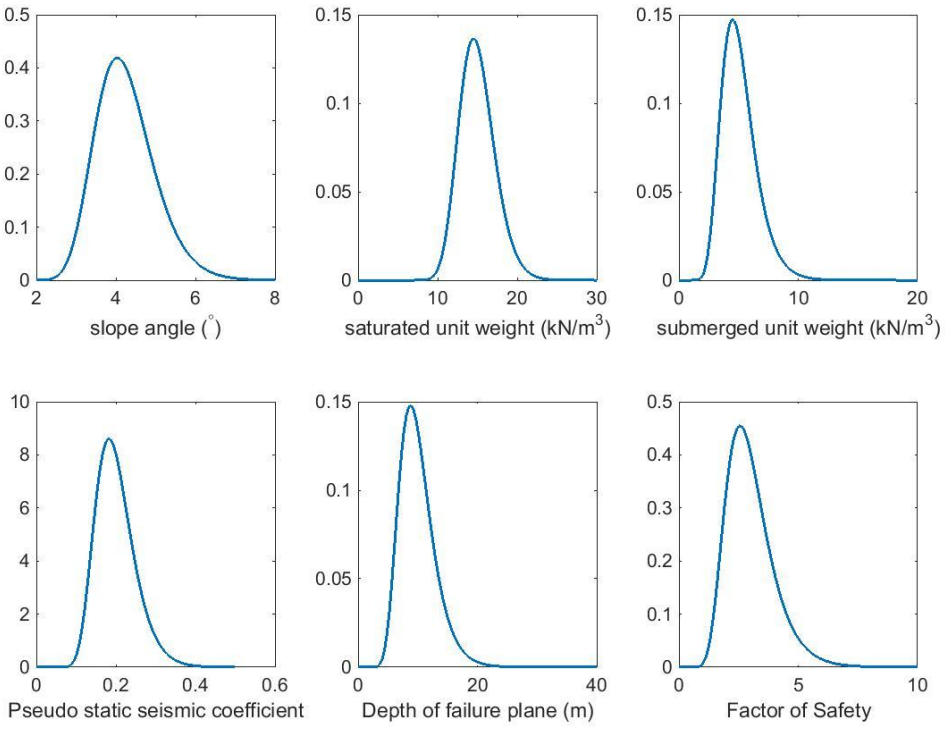

Fig. 3.1. Prior probability density functions of the model parameters.

3.3 Likelihood Function

The likelihood function is assumed to be following a Gaussian distribution. The mean equals the model prediction with the proposed values of the model parameters and variance equal to the variance of the experimental data. It is given as follows.

$$P(dobs|g(\theta)) = P(dobs_1|g(\theta)) * P(dobs_2|g(\theta)) \ldots * P(dobs_n|g(\theta))$$

$$P(dobs|g(\theta)) = \Pi P(dobs|g(\theta))$$

Where,

$$dobs_n = number\ of\ experimental\ data\ points.$$

$$g(\theta) = Infinite\ slope\ model$$

$$\theta = Vector\ of\ random\ parameters$$

3.4 Experimental Design

The experimental design is divided into two parts as shown in the tables 3.2 and 3.3. Experiment 1 calculates the probability of failure of the slope in limit state condition with factor of safety equals unity whereas experiment 2 considers factor of safety as a random variable. The factor of safety was incorporated into the infinite slope model as measure of caution with the model predictions owning to its simplicity. The mobilized shear strength predictions with factor of safety as a random variable were more conservative when compared to the model predictions with factor of safety equaled unity. Hence there are totally 24 cases with varying amount of experimental data and prior information of model parameter (slope angle) for which the probability of failure is calculated. The thesis presents the results of four cases as highlighted in tables 3.2 and 3.3. Generally the slope angles are derived from digital elevation models using the

ArcGIS software. Therefore the access to the bathymetry data of the area provides greater information about the slope parameter in terms of more accurate estimates of slope angle

FS	LIMIT STATE (Factor of Safety = 1)											
NO OF POINTS	5						20					
PRIOR	INFORMATIVE (on slope angle α)						INFORMATIVE(on slope angle α)					
SLOPE ANGLE	5	15	25	35	45	55	5	15	25	35	45	55

Table 3.2. Factor of safety equals unity.

FS	Factor of Safety = RANDOM VARIABLE											
NO OF POINTS	5						20					
PRIOR	INFORMATIVE(on slope angle α)						INFORMATIVE(on slope angle α)					
SLOPE ANGLE	5	15	25	35	45	55	5	15	25	35	45	55

Table 3.3. Factor of safety as a random variable.

3.4.1 Experimental Observations

The 5 and 20 experimental observations of undrained shear strength were synthetically generated with the help of a random number generator from a log-normal distribution with a mean of 125 kN/m^3 and variance of 625 kN/m^3 as shown in figure 3.2.

a)

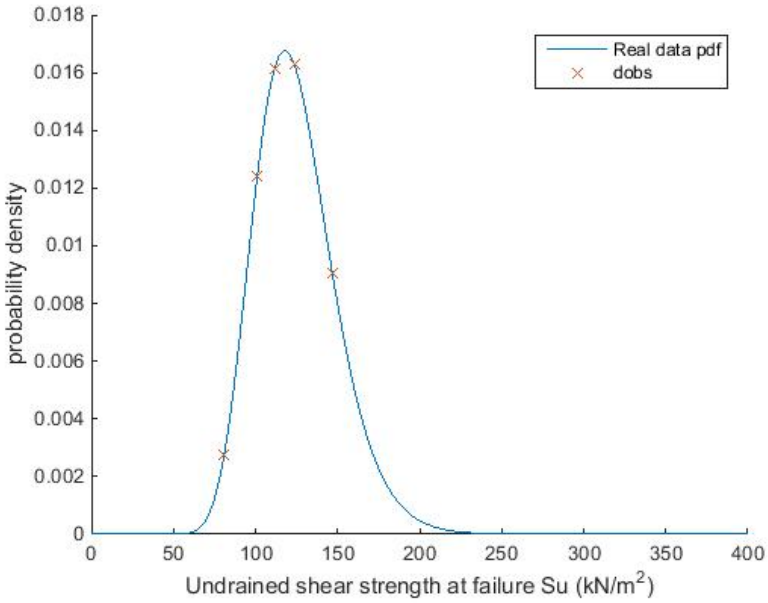

Fig. 3.2. Randomly generated data. Experimental observations are synthetically generated from a log-normal distribution with a mean of 125 kN/m^2 and a variance of 625 kN/m^2. (a) The case of 5 experimental observations randomly sampled from the distribution. (b) The case of 20 experimental observations randomly sampled from the distribution.

b)

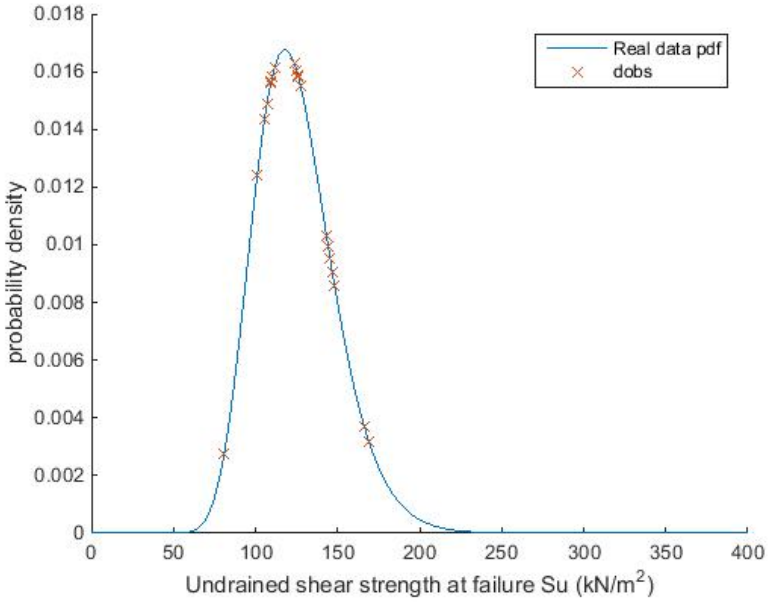

Fig. 3.2 Continued.

4. RESULTS

4.1. Case I: Factor of Safety Equals Unity, 5 Experimental Observations

In this case 5 experimental observations were synthetically generated and used for the calibration of the infinite slope model using the Bayesian inference.

The figure 4.1 show the sequence of 600000 samples generated from the posterior distributions of the model parameters and their respective cumulative mean and standard deviation using the MCMC-Metropolis algorithm. The cumulative mean and standard deviation converged after 200000 iterations, therefore the burn in point was chosen to be at 200000. The sequence of samples from 200001 to 600000 for each parameter were used to run the forward simulations of the infinite slope model to estimate the mean and the variance of the model predictions.

a)

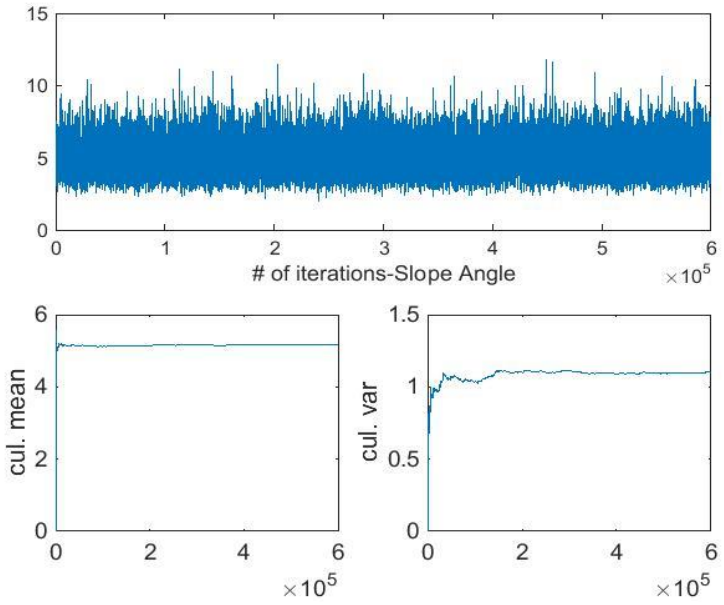

b)

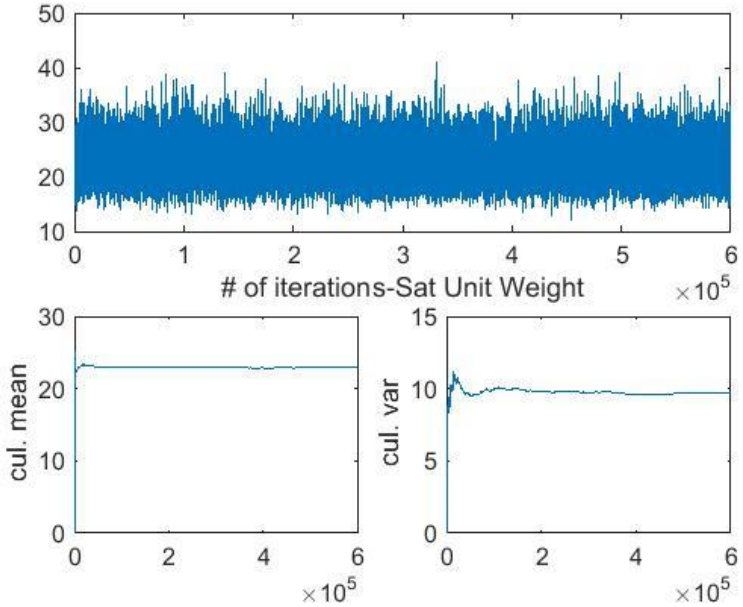

Fig. 4.1. Convergence plots of model parameters for Case I. (a) Slope angle. (b) Saturated unit weight. (c) Submerged unit weight. (d) Depth of failure plane. (e) Pseudo static seismic coefficient.

c)

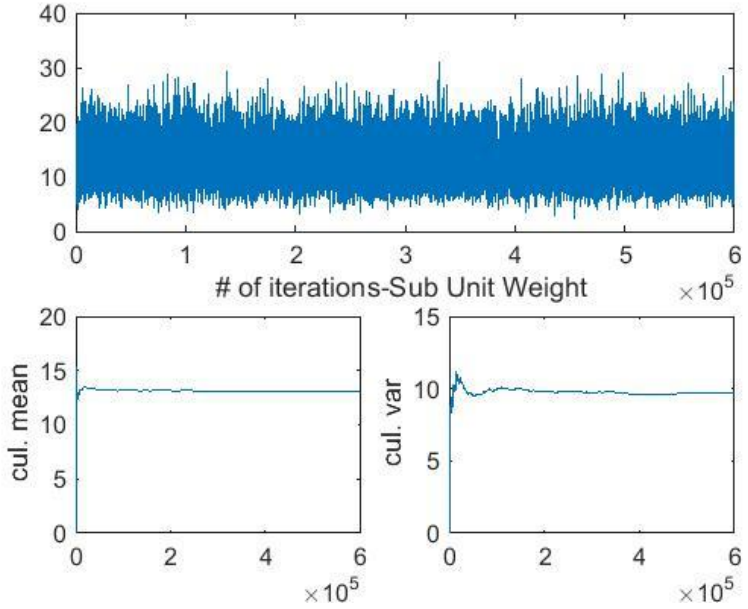

d)

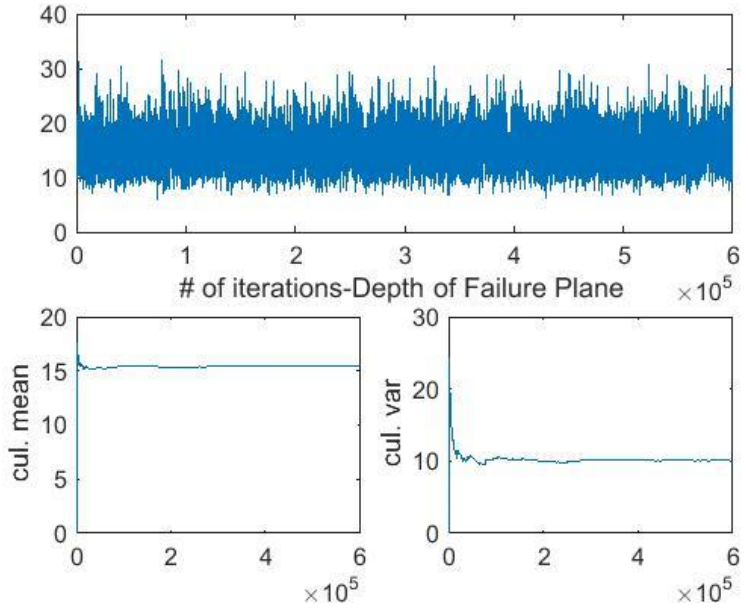

Fig. 4.1. Continued.

e)

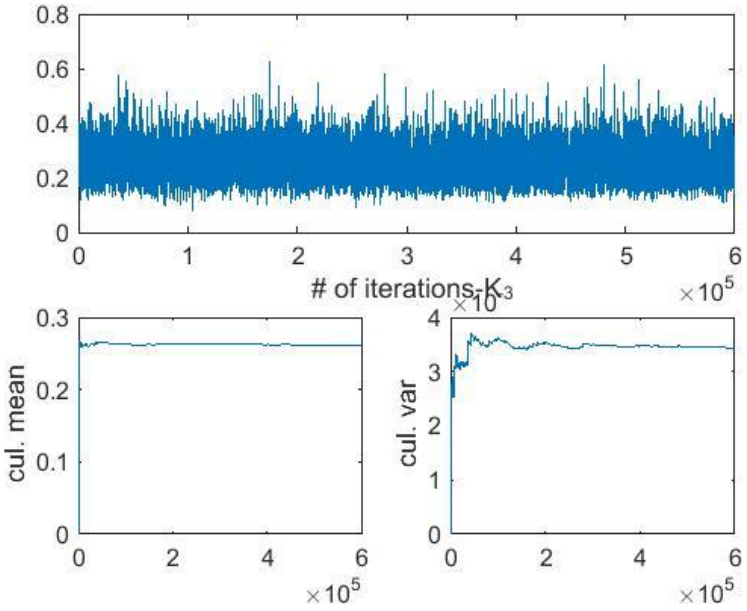

Fig. 4.1. Continued.

The Bayesian inference updated the initial state of evidence (prior distributions) about the model parameters after the calibration of the infinite slope model with 5 experimental observations. The change in the distributions of each model parameters is shown in figures 4.2 as a comparison between their prior and posterior empirical cumulative distribution functions. The sequence of samples after the burn in point of 200000 were used to generate the empirical cumulative distribution function for the posterior distribution for each model parameters. Significant increase in the distribution of the unit weight, depth of failure and pseudo static seismic coefficient were observed. The initial state of evidence about the unit weight, depth of failure plane were non conservative in estimating the mobilized shear strength of the soil.

a)

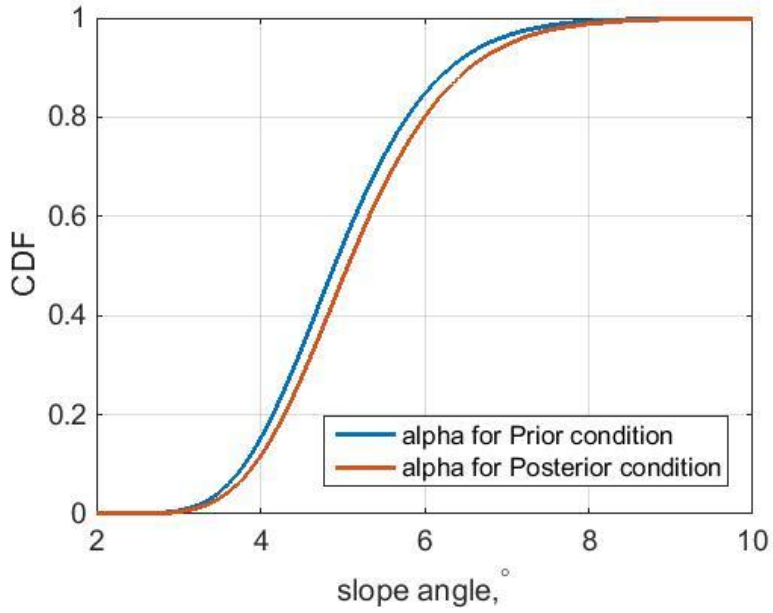

b)

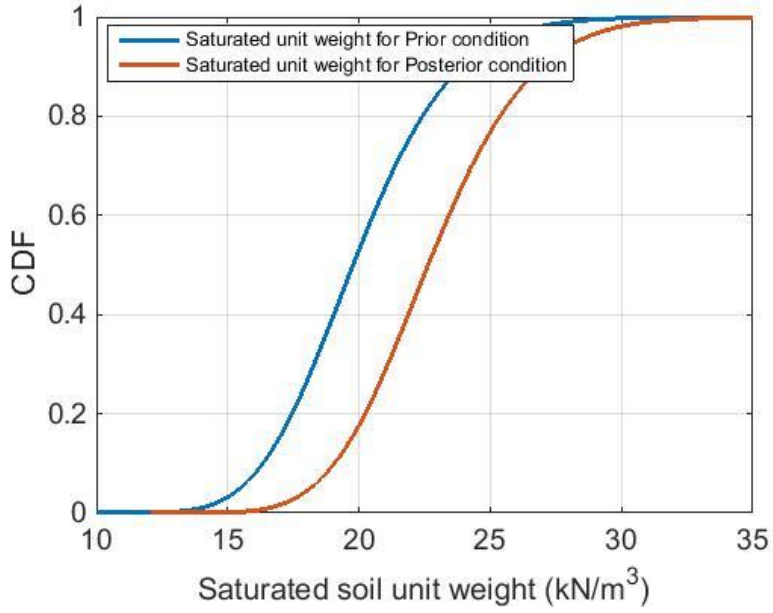

Fig. 4.2. Empirical CDFs of posterior vs prior distributions of the model parameters for Case I. (a) Slope angle. (b) Saturated unit weight. (c) Submerged unit weight. (d) Depth of failure plane. (e) Pseudo static seismic coefficient.

c)

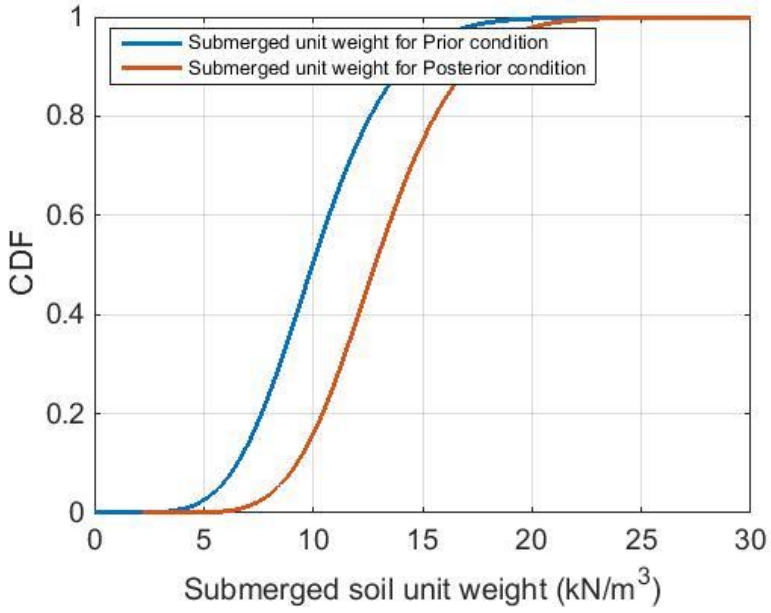

d)

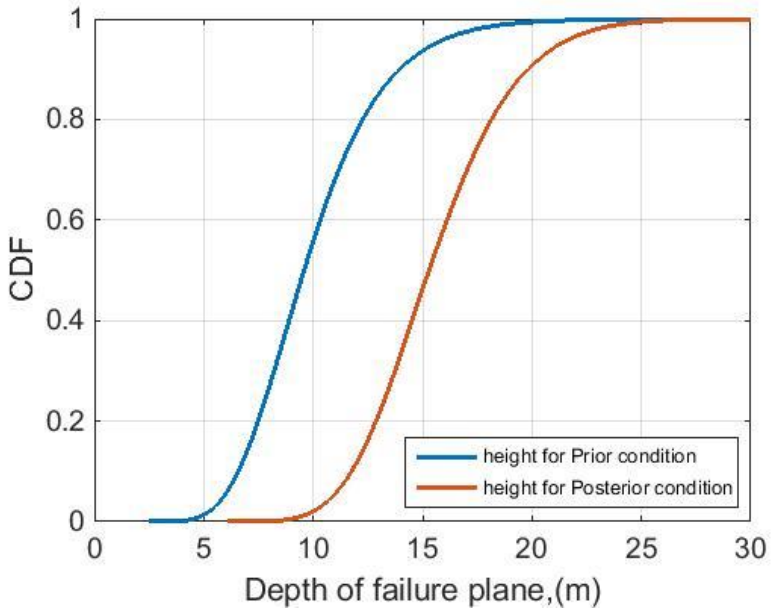

Fig. 4.2. Continued.

e)

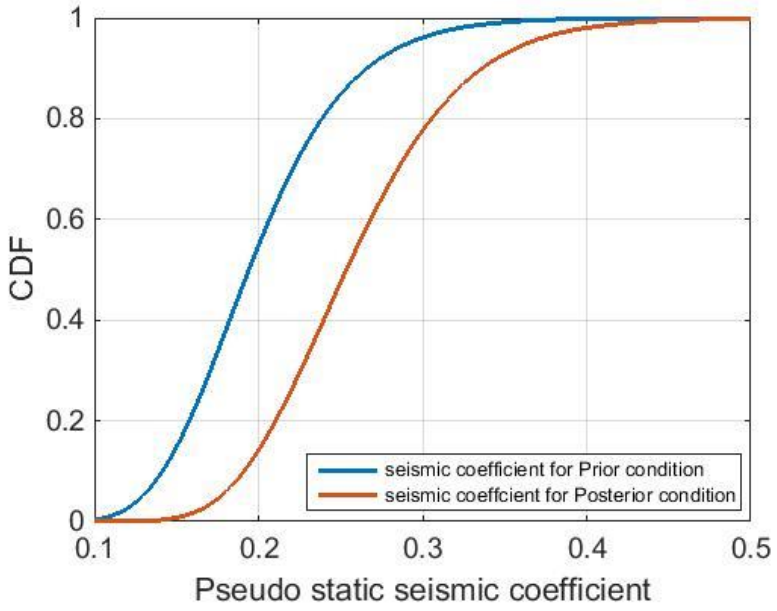

Fig. 4.2. Continued.

The model predictions on the undrained shear strength sampled from the prior distributions and posterior distributions of the model parameters are compared with real data on the undrained shear strength of the soil. The model predictions are represented as their probability density functions. The log normal distribution with mean 125 kN/m^3 and variance 625 kN/m^3 from which the experimental observations (5 points) were sampled represents the real in-situ undrained shear strength of the soil. The mean and standard deviation of the model predictions are tabulated in table 4.1, figure 4.3 and 4.4. The results showed greater certainty in the model predictions when sampled from the posterior as could be exemplified by reduction in the standard deviation. The mean of

the model predictions were much closer to the mean of the real in-situ undrained shear strength of the soil.

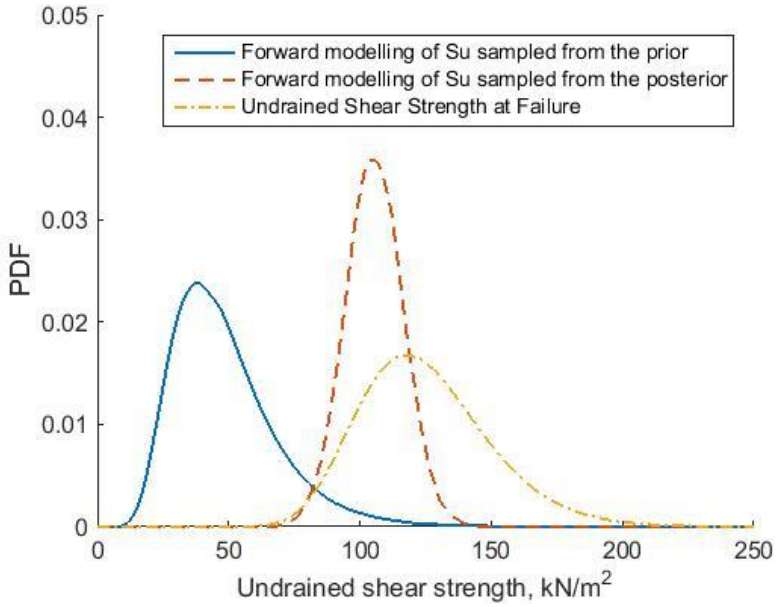

Fig. 4.3. Comparison of model predictions between the experimental data, forward modelling from prior distributions and forward modelling from posterior distributions for Case I.

Estimates	Prior		Posterior	
	Mean	Std	Mean	Std
Prediction of mobilized Shear Strength (kN/m2)	49	19.239	105.003	11.036

Table 4.1. Comparison of first order statistics for Case I.

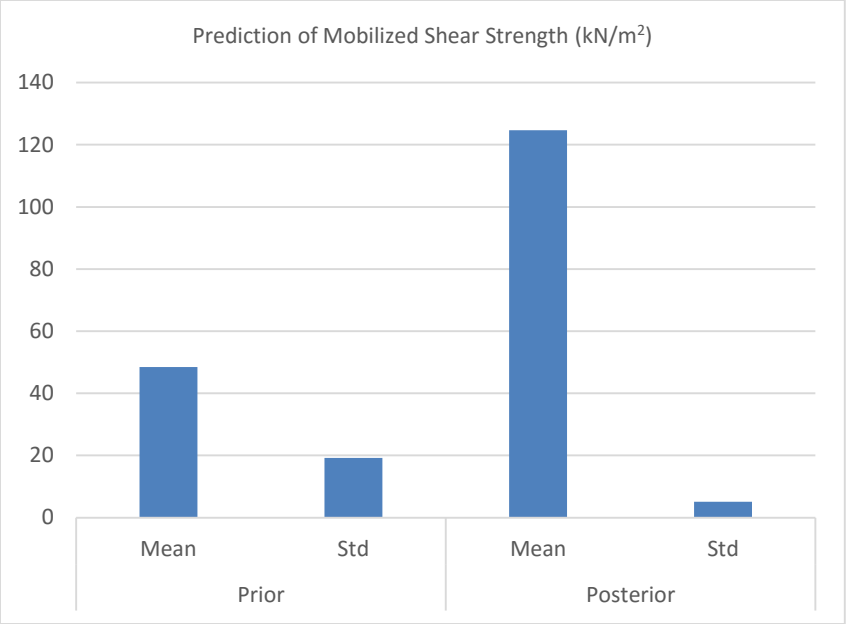

Fig. 4.4. Bar chart of the first order statistics for Case I.

The gain in the level of certainty in the model predictions resulted in increase in the estimates of the probability of failure as shown in table 4.2. Figure 4.4 shows the first order statistics for Case I.

Estimate	Prior	Posterior
Probability of Failure (%)	4.057	28.664

Table 4.2. Estimates of probability of failure for Case I.

The Bayesian inference for the calibration of the infinite slope model indicated a correlation structure among the model parameters which were initially assumed to be

uncorrelated. Figure 4.5 shows the joint probability histograms between the model parameters. Table 4.3 presents the values of the correlation coefficients between the model parameters. The model parameters were initially considered as uncorrelated. A negative correlation between saturated unit weight and depth of failure plane was indicated.

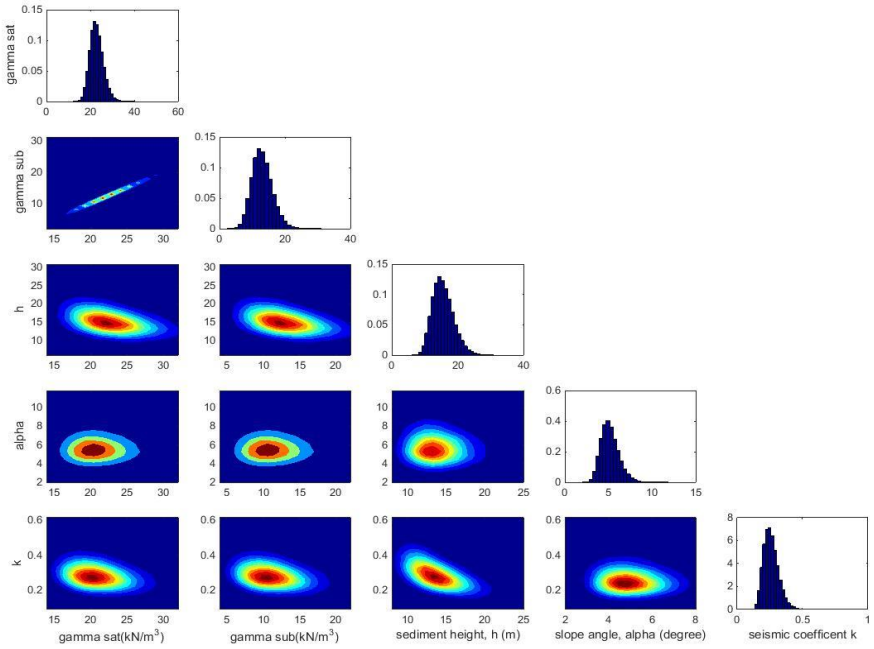

Fig. 4.5. Joint probability histograms of the model parameters for Case I.

Model Parameters	Sat Unit Weight	Sub Unit Weight	Depth	Slope Angle	Seismic Coeff.
Sat Unit Weight	1.0000	1.0000	-0.4227	-0.0094	-0.2714
Sub Unit Weight	1.0000	1.0000	-0.4227	-0.0094	-0.2714
Depth	-0.4227	-0.4227	1.0000	-0.0725	-0.5750
Slope Angle	-0.0094	-0.0094	-0.0725	1.0000	-0.0702
Seismic Coeff.	-0.2714	-0.2714	-0.5750	-0.0702	1.0000

Table 4.3. Correlation coefficients between the model parameters for Case I.

The results presented above were for the case where the prior distribution of the slope angle was centered about 5° with a variance of 1°. Similar analysis were conducted for various angles and the summary of change in the posterior distributions of each model parameter with varying slope angle are presented in figure 4.6.

a)

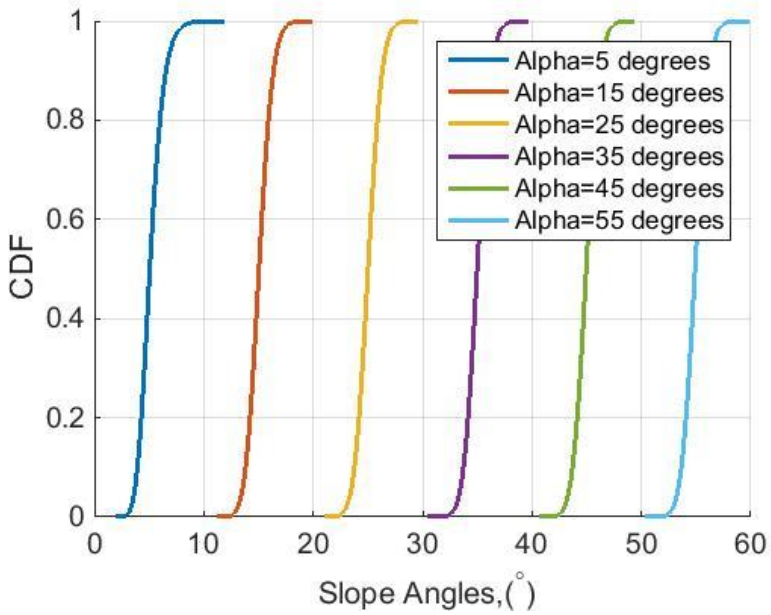

Fig. 4.6. Empirical CDFs of posterior distributions with varying slope angles for Case I. (a) Slope angle. (b) Saturated unit weight. (c) Depth of failure plane. (d) Pseudo static seismic coefficient.

b)

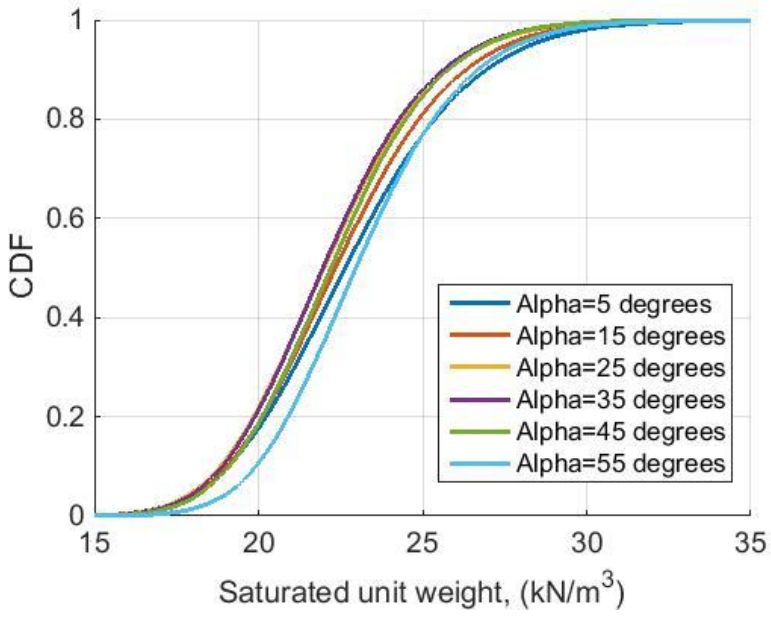

c)

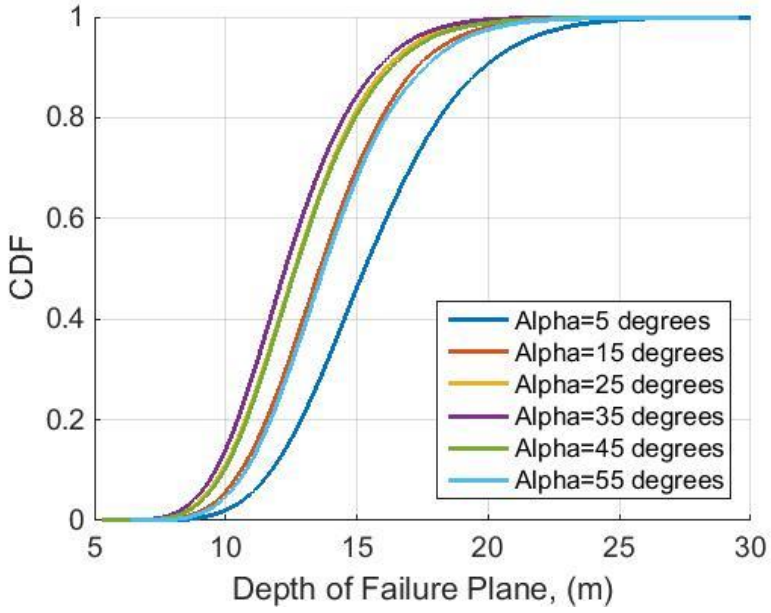

Fig. 4.6. Continued.

d)

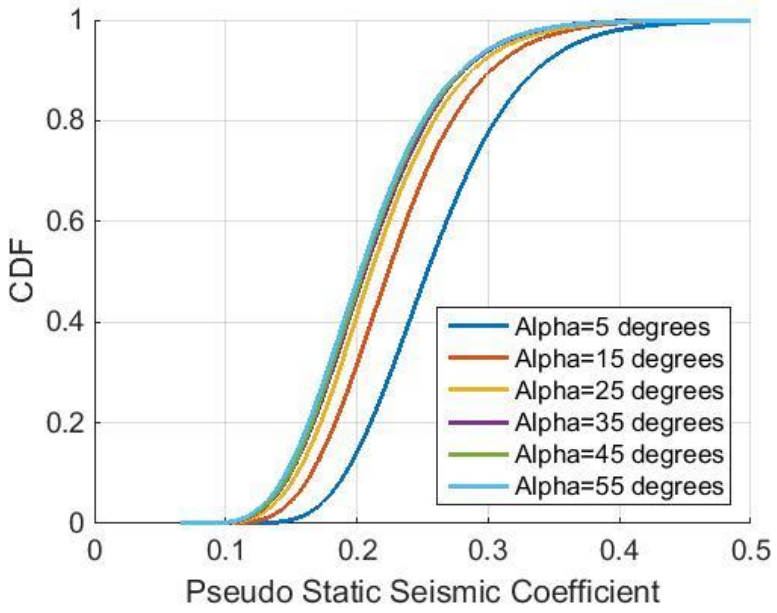

Fig. 4.6. Continued.

4.2. Case II: Factor of Safety Equals Unity, 20 Experimental Observations

In this case 20 experimental observations were synthetically generated and used for the calibration of the infinite slope model using the Bayesian inference. The figure 4.7 shows the sequence of 600000 samples generated from the posterior distributions of the model parameters and their respective cumulative mean and standard deviation using the MCMC-Metropolis algorithm. The cumulative mean and standard deviation converged after 200000 iterations, therefore the burn in point was chosen to be at 200000. The sequence of samples from 200001 to 600000 for each parameter were used to run the forward simulations of the infinite slope model to estimate the mean and the variance of the model predictions.

a)

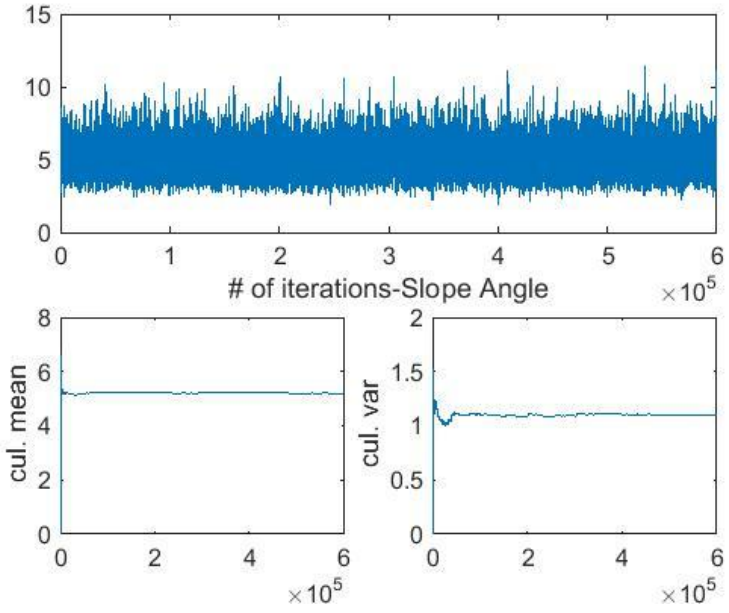

b)

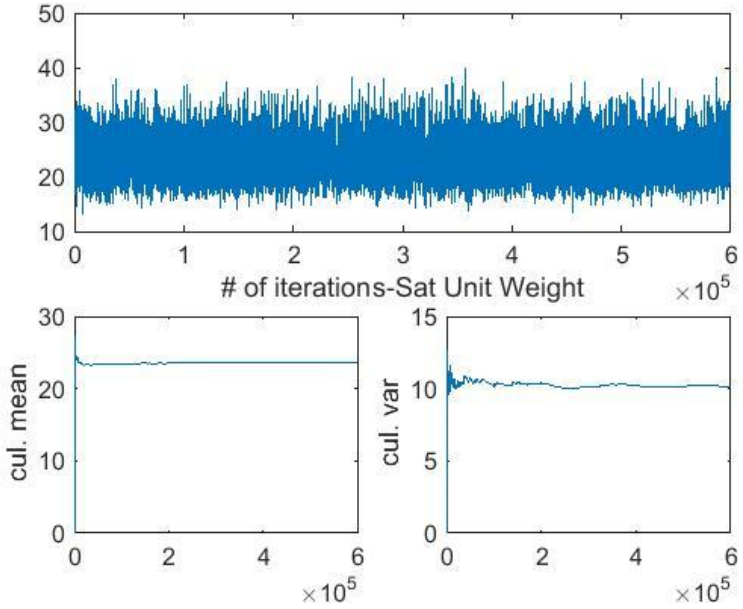

Fig. 4.7. Convergence plots of model parameters for Case II. (a) Slope angle. (b) Saturated unit weight. (c) Submerged unit weight. (d) Depth of failure plane. (e) Pseudo static seismic coefficient.

c)

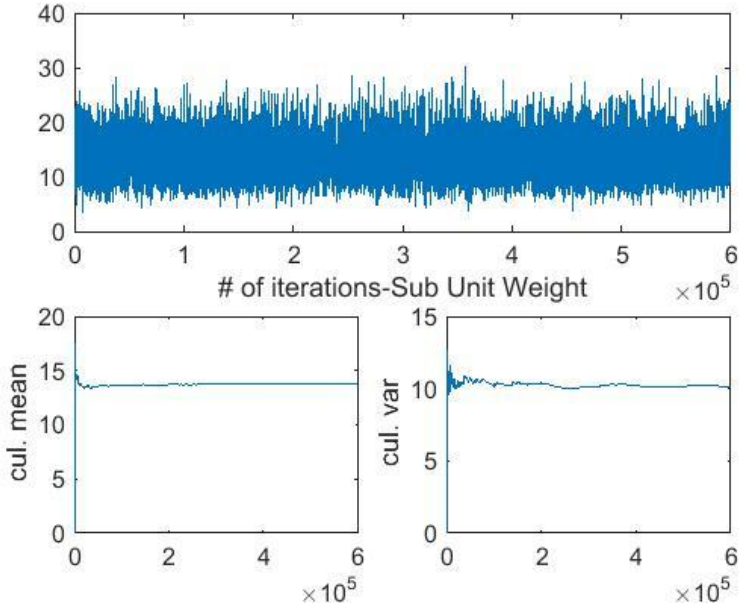

d)

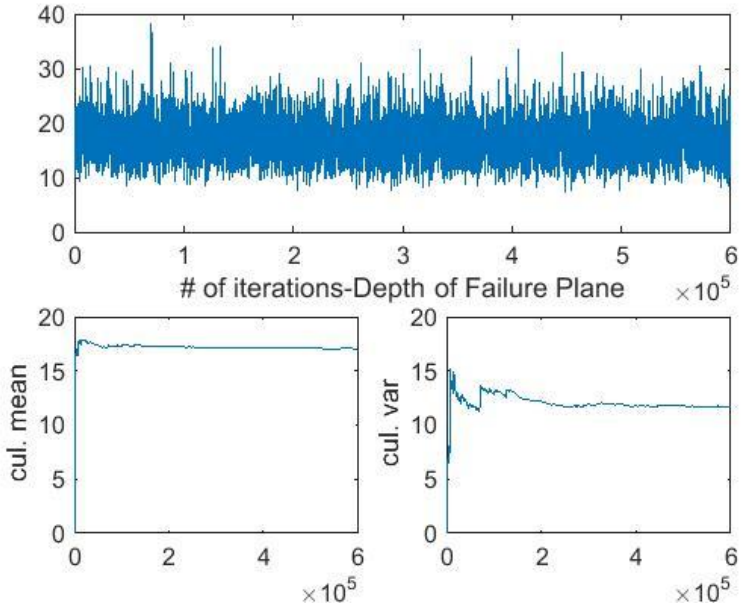

Fig. 4.7. Continued.

e)

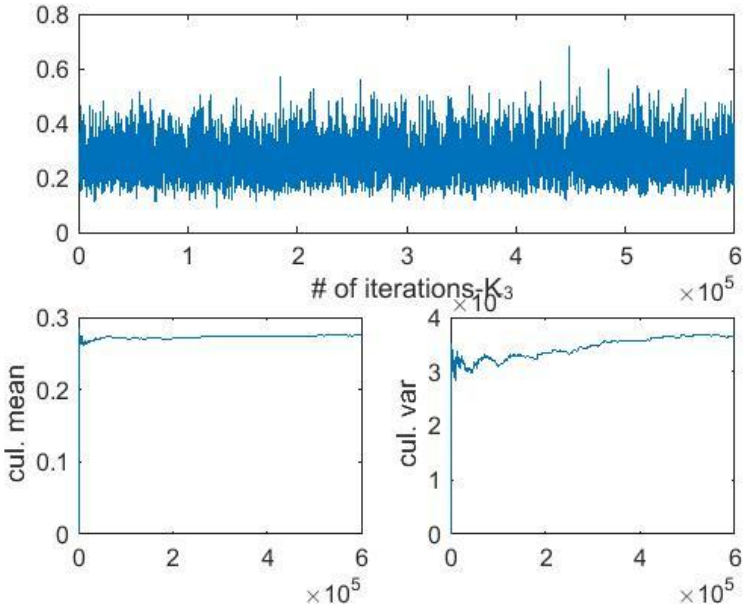

Fig. 4.7. Continued

The Bayesian inference updated the initial state of evidence (prior distributions) about the model parameters after the calibration of the infinite slope model with 20 experimental observations. The change in the distributions of each model parameters is shown in figure 4.8 as a comparison between their prior and posterior empirical cumulative distribution functions. The sequence of samples after the burn in point of 200000 were used to generate the empirical cumulative distribution function for the posterior distribution for each model parameters. Similar to Case I (calibration with 5 experimental observations) significant increase in the distribution of the unit weight, depth of failure and pseudo static seismic coefficient were observed. The initial state of

evidence about the unit weight, depth of failure plane were non conservative in estimating the mobilized shear strength of the soil.

a)

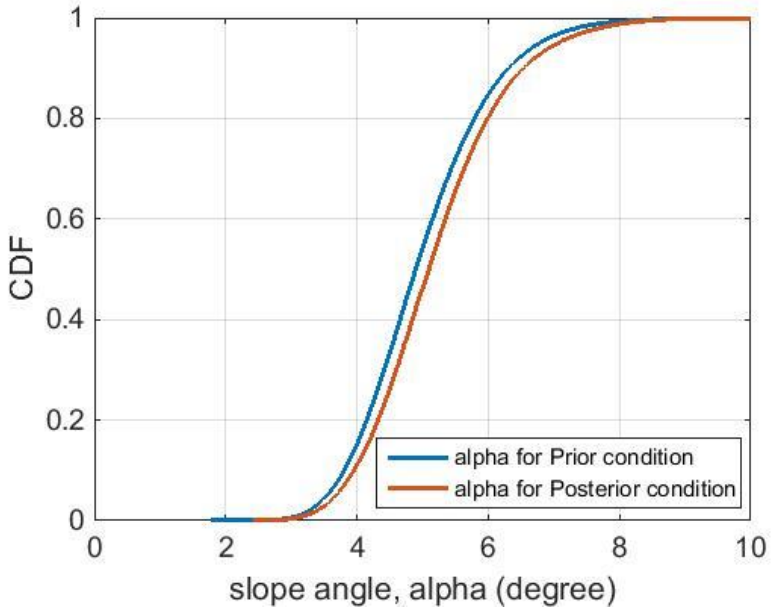

Fig. 4.8. Empirical CDFs of posterior vs prior distributions of the model parameters for Case II. (a) Slope angle. (b) Saturated unit weight. (c) Submerged unit weight. (d) Depth of failure plane. (e) Pseudo static seismic coefficient.

b)

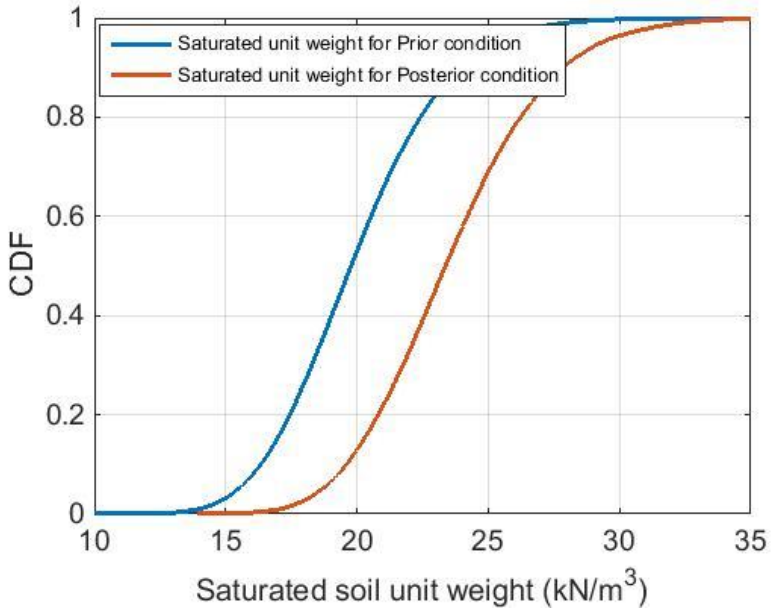

c)

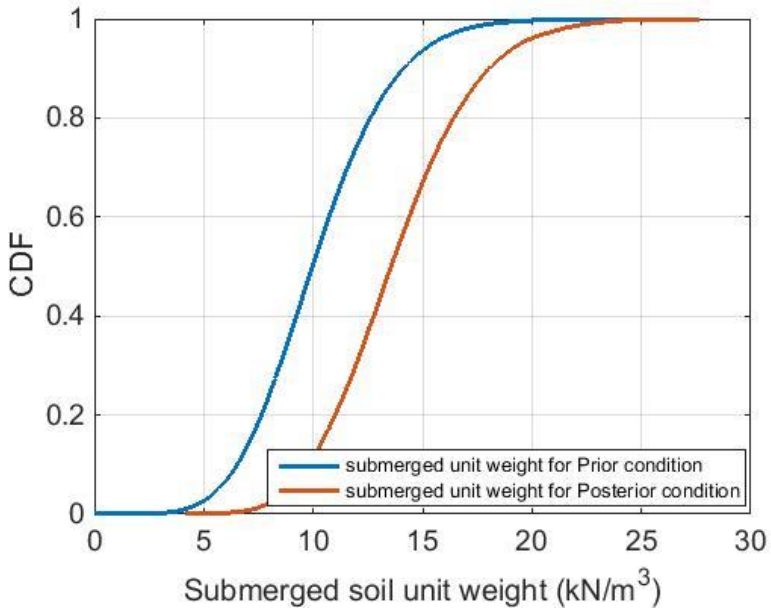

Fig. 4.8. Continued.

d)

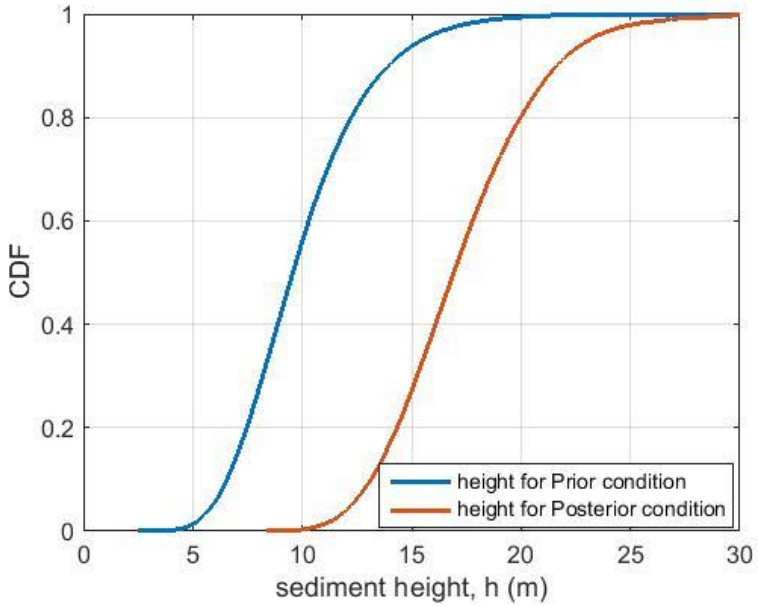

e)

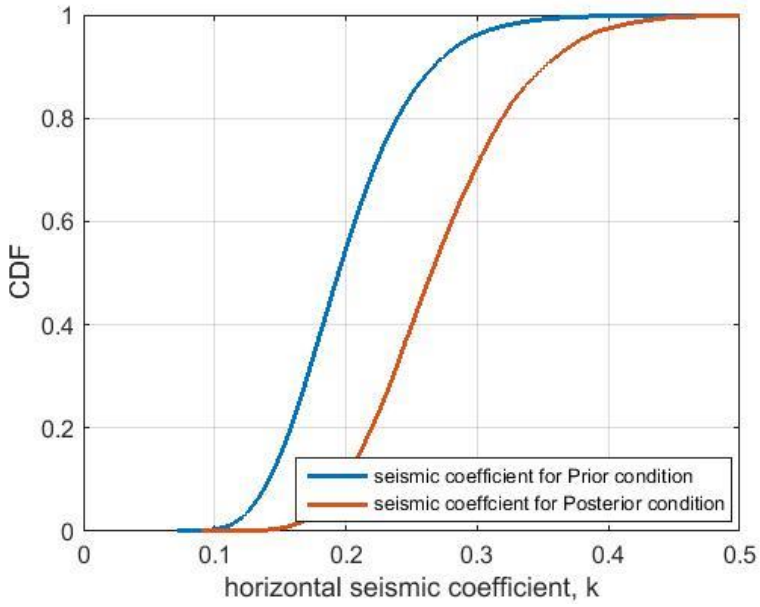

Fig. 4.8. Continued.

The model predictions on the undrained shear strength sampled from the prior distributions and posterior distributions of the model parameters are compared with real data on the undrained shear strength of the soil. The model predictions are represented as their probability density functions. The log normal distribution with mean 125 kN/m^3 and variance 625 kN/m^3 from which the experimental observations (20 points) were sampled represents the real in-situ undrained shear strength of the soil. The mean and standard deviation of the model predictions are tabulated in table 4.4 and figures 4.9 & 4.10. Compared to Case I (calibration with 5 experimental observations) the results showed greater reduction in the standard deviation of the model predictions when sampled from the posterior. The mean of the model predictions very nearly captures the mean of the real in-situ undrained shear strength of the soil. Incorporating greater amount of experimental observations (5 points to 20 points) greatly increased the certainty and accuracy of the model predictions.

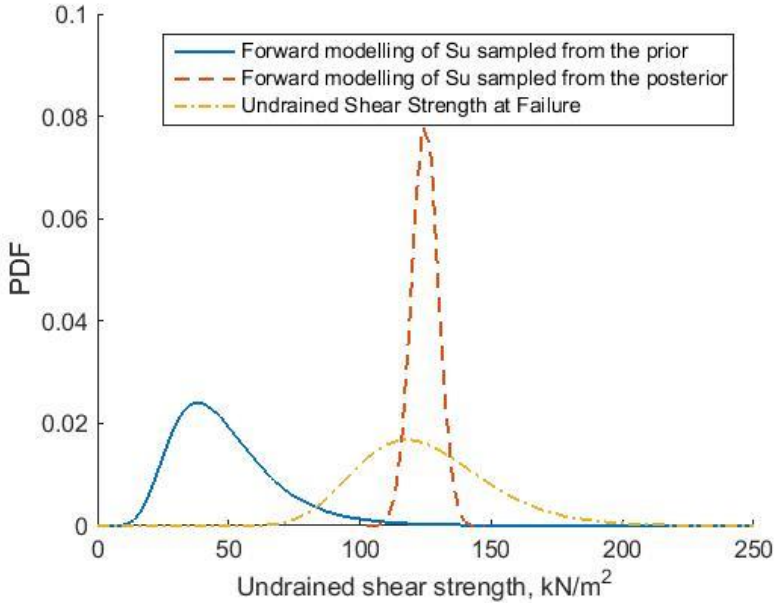

Fig. 4.9. Comparison of model predictions between the experimental data, forward modelling from prior distributions and forward modelling from posterior distributions for Case II.

Estimates	Prior		Posterior	
	Mean	Std	Mean	Std
Prediction of mobilized Shear Strength (kN/m2)	48	19.208	124.69	5.088

Table 4.4. Comparison of first order statistics for Case II.

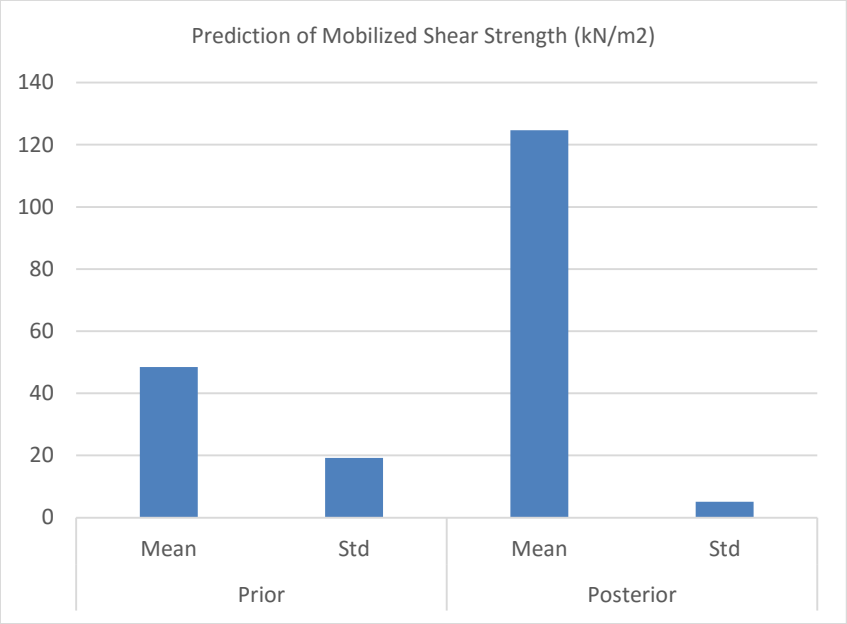

Fig. 4.10. Bar chart of the first order statistics for Case II.

Estimate	Prior	Posterior
Probability of Failure (%)	4.057	49.637

Table 4.5. Estimates of probability of failure for Case II.

Increase in the estimate of probability of failure towards the actual probability of failure is observed with greater certainty on the model predictions as shown in table 4.5.

The Bayesian inference for the calibration of the infinite slope model indicated a correlation structure among the model parameters which were initially assumed to be uncorrelated. Figure 4.11 shows the joint probability histograms between the model

parameters. Table 4.6 presents the values of the correlation coefficients between the model parameters.

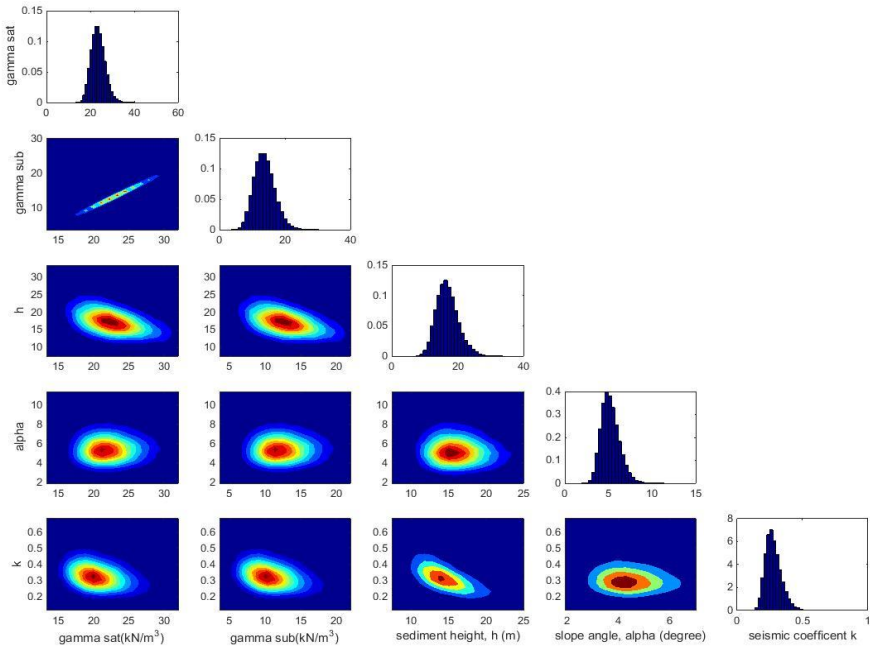

Fig. 4.11. Joint probability histograms of the model parameters for Case II.

Model Parameters	Sat Unit Weight	Sub Unit Weight	Depth	Slope Angle	Seismic Coeff.
Sat Unit Weight	1.0000	1.0000	-0.4627	0.0076	-0.2963
Sub Unit Weight	1.0000	1.0000	-0.4627	0.0076	-0.2963
Depth	-0.4627	-0.4627	1.0000	-0.0815	-0.6419
Slope Angle	0.0076	0.0076	-0.0815	1.0000	-0.0792
Seismic Coeff.	-0.2963	-0.2963	-0.6419	-0.0792	1.0000

Table 4.6. Correlation coefficients between the model parameters for Case II.

The results presented above were for the case where the prior distribution of the slope angle was centered about 5° with a variance of 1°. Similar analysis were conducted for various angles and the summary of change in the posterior distributions of each model parameter with varying slope angle are presented in figure 4.12.

a)

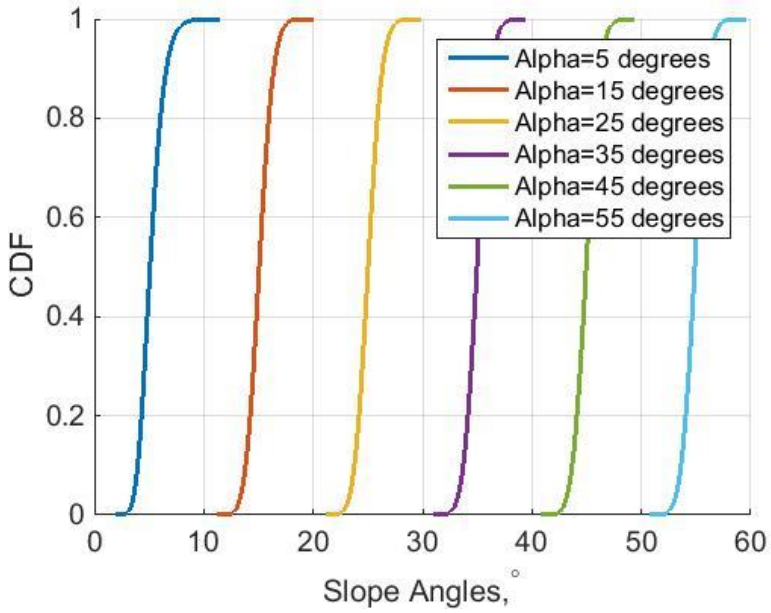

Fig. 4.12. Empirical CDFs of posterior distribution with varying slope angles for Case II (a) Slope angle. (b) Saturated unit weight. (c) Depth of failure plane. (d) Pseudo static seismic coefficient.

b)

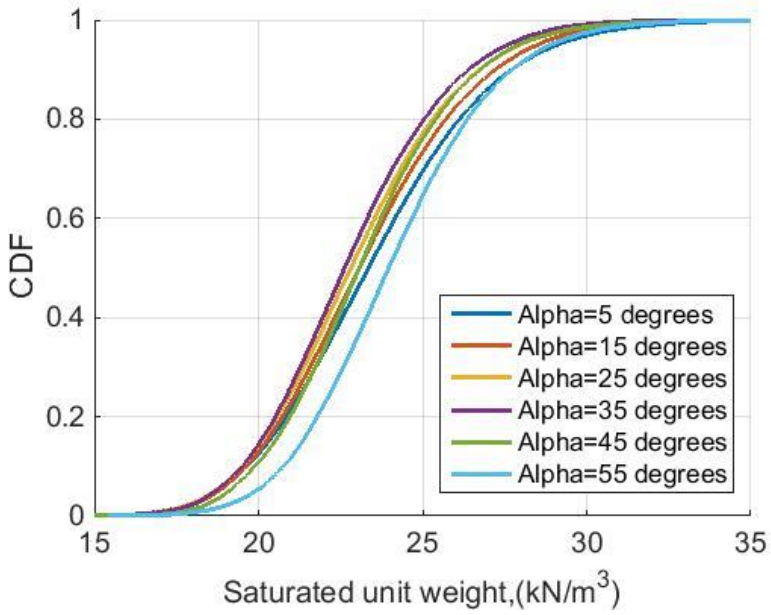

c)

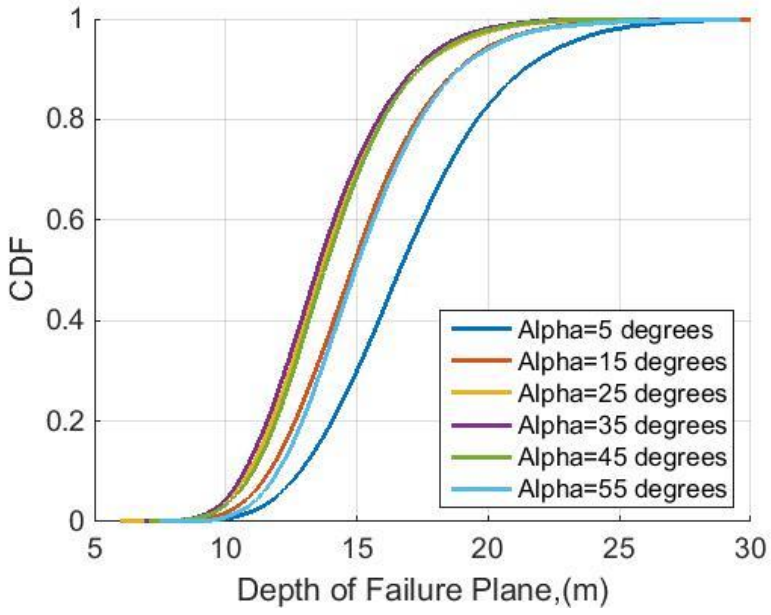

Fig. 4.12. Continued.

d)

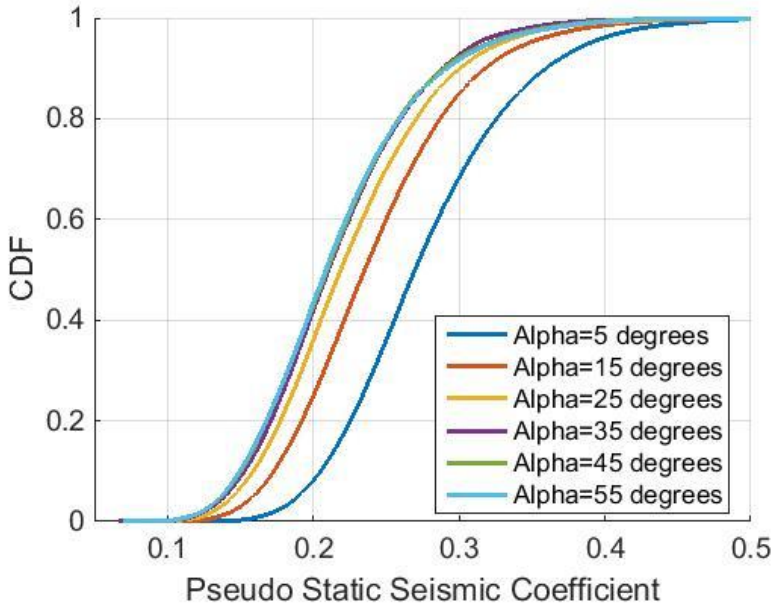

Fig. 4.12. Continued.

4.3. Case III: Factor of Safety Equals Random Variable, 5 Experimental Observations

In this case factor of safety was considered as a random variable and 5 experimental observations were synthetically generated and used for the calibration of the infinite slope model using the Bayesian inference. The factor of safety was incorporated into the infinite slope model as measure of caution with the model predictions owning to its simplicity. The mobilized shear strength predictions with factor of safety as a random variable were more conservative when compared to the model predictions with factor of safety equaled unity.

The figure 4.13 show the sequence of 600000 samples generated from the posterior distributions of the model parameters and their respective cumulative mean and

standard deviation using the MCMC-Metropolis algorithm. The cumulative mean and standard deviation converged after 200000 iterations, therefore the burn in point was chosen to be at 200000. The sequence of samples from 200001 to 600000 for each parameter were used to run the forward simulations of the infinite slope model to estimate the mean and the variance of the model predictions.

a)

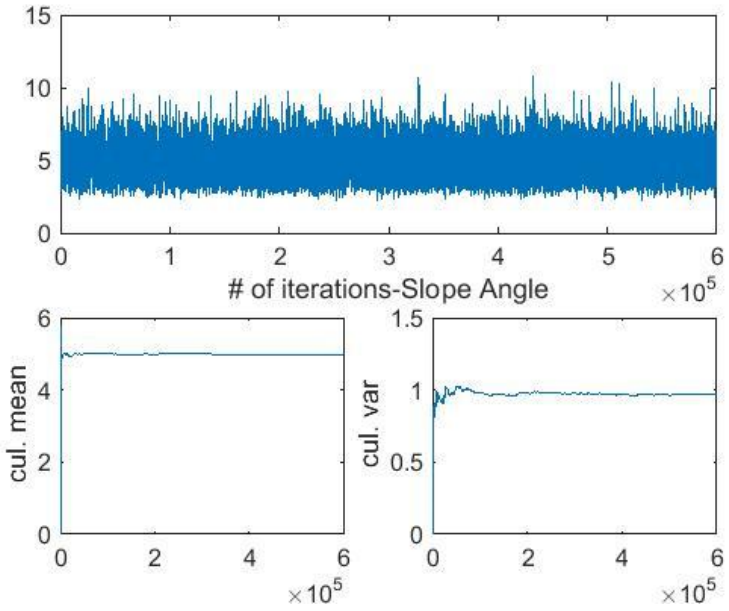

Fig. 4.13. Convergence plots of model parameters for Case III. (a) Slope angle. (b) Saturated unit weight. (c) Submerged unit weight. (d) Depth of failure plane. (e) Pseudo static seismic coefficient. (f) Factor of Safety.

b)

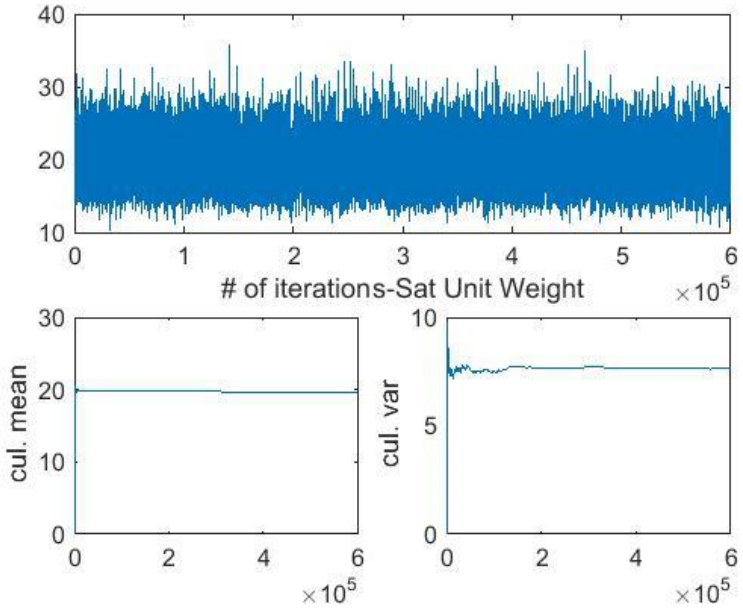

c)

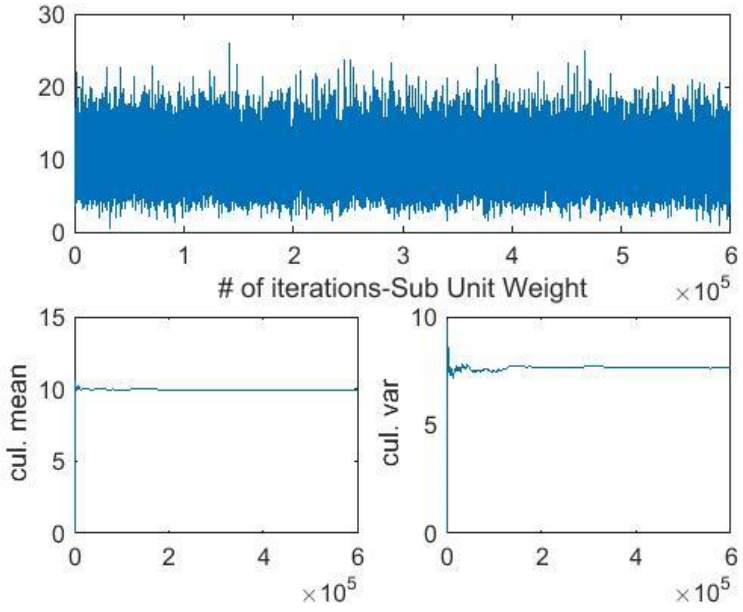

Fig. 4.13. Continued.

d)

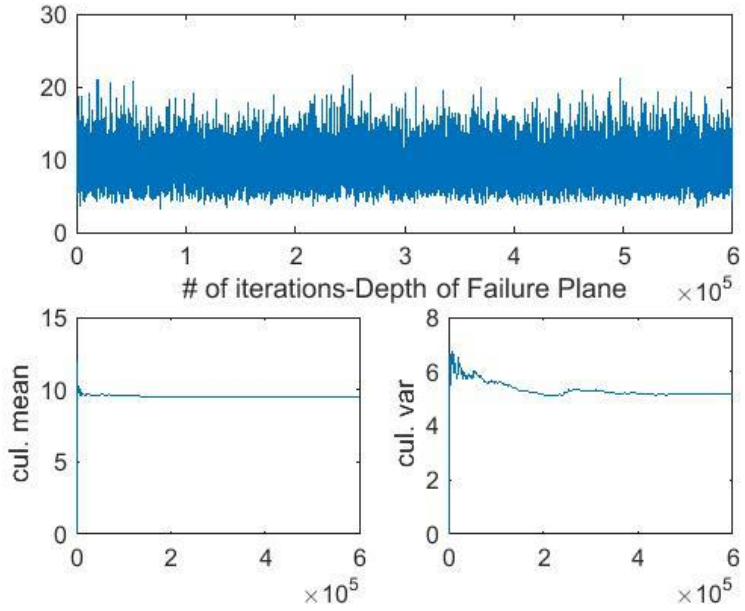

e)

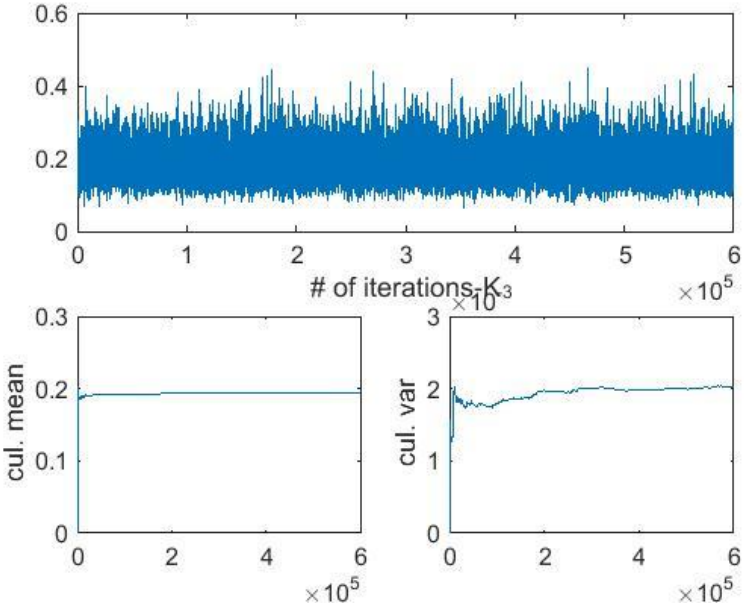

Fig. 4.13. Continued.

f)

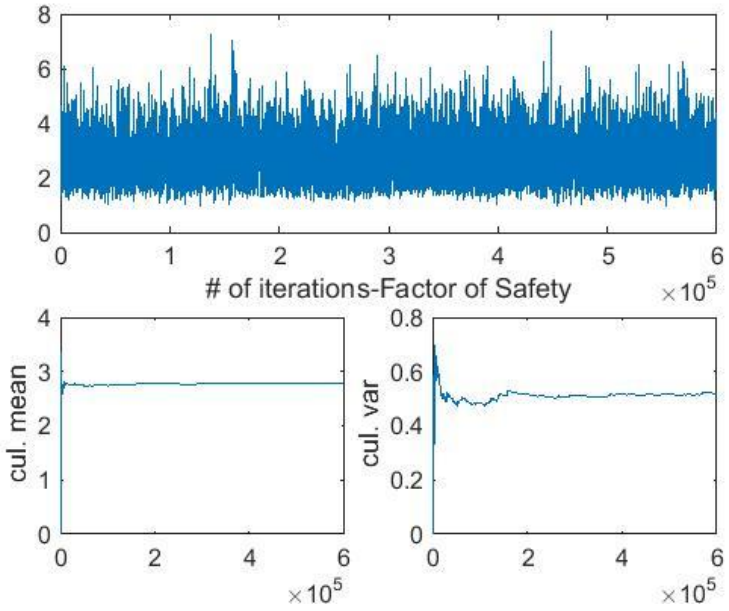

Fig. 4.13. Continued.

The Bayesian inference updated the initial state of evidence (prior distributions) about the model parameters after the calibration of the infinite slope model with 5 experimental observations. The change in the distributions of each model parameters is shown in figure 4.14 as a comparison between their prior and posterior empirical cumulative distribution functions. The sequence of samples after the burn in point of 200000 were used to generate the empirical cumulative distribution function for the posterior distribution for each model parameters. Very slight changes in the distributions of model parameters were observed. However, there were noticeable changes on the distributions of Depth of Failure plane and the Factor of safety.

a)

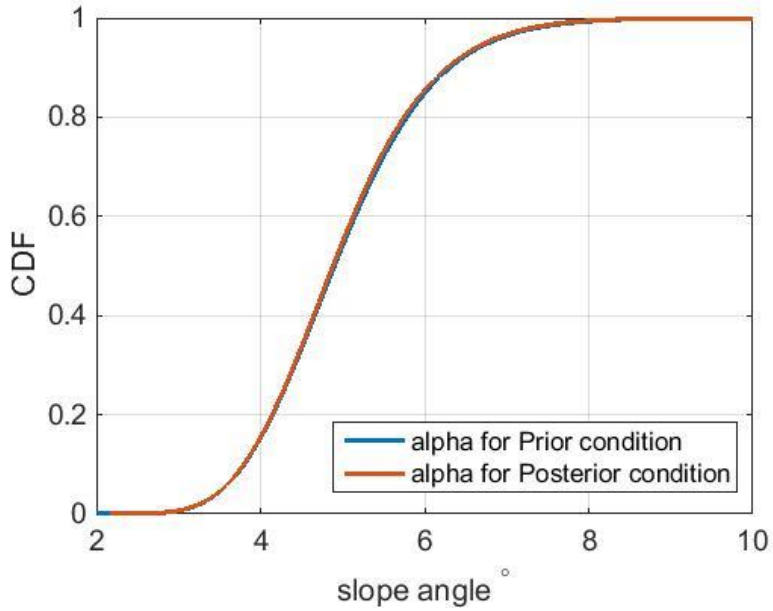

b)

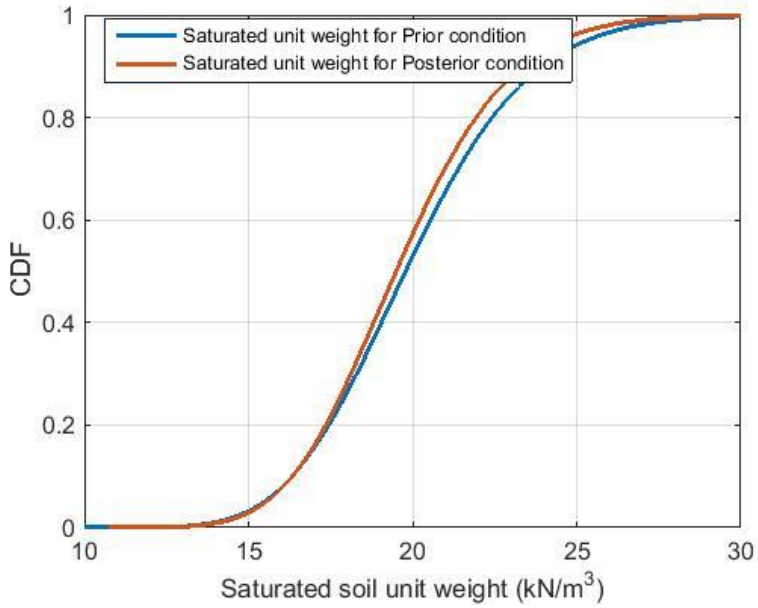

Fig. 4.14. Empirical CDFs of posterior vs prior distributions of the model parameters for Case III. (a) Slope angle. (b) Saturated unit weight. (c) Submerged unit weight. (d) Depth of failure plane. (e) Pseudo static seismic coefficient. (f) Factor of Safety.

c)

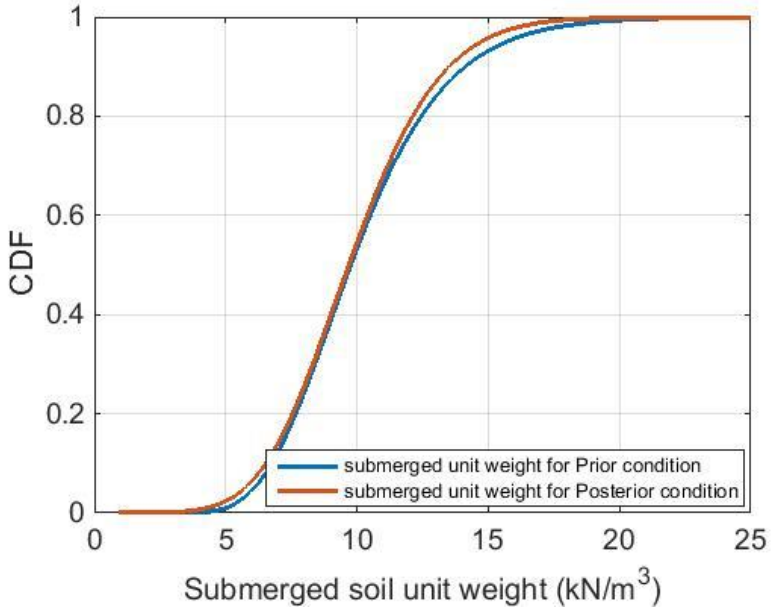

d)

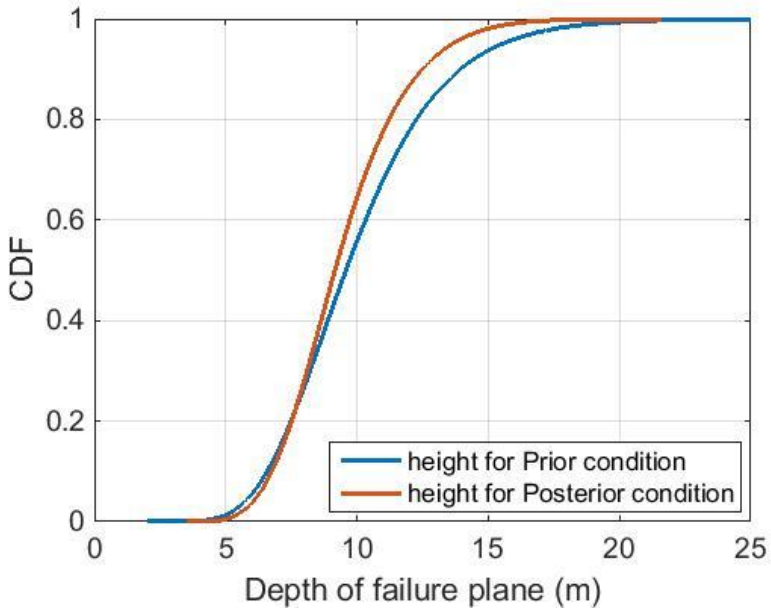

Fig. 4.14. Continued.

e)

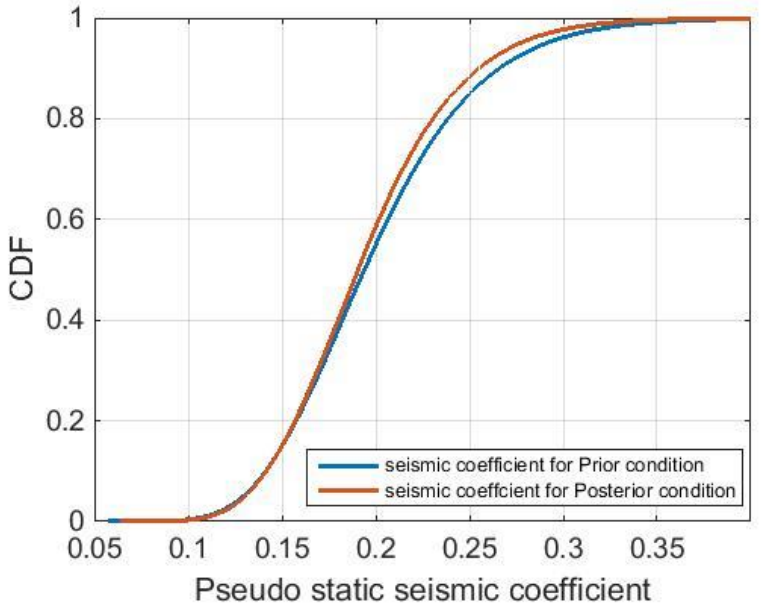

f)

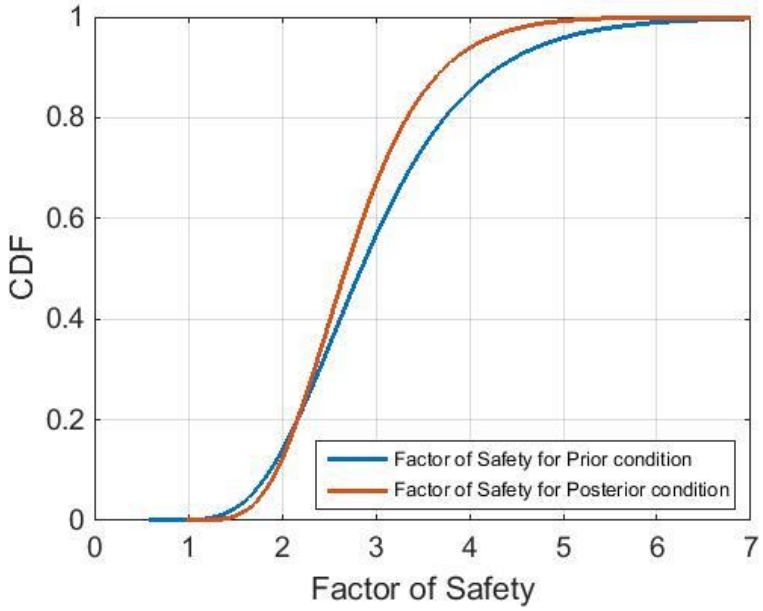

Fig. 4.14. Continued.

The model predictions on the undrained shear strength sampled from the prior distributions and posterior distributions of the model parameters are compared with real data on the undrained shear strength of the soil. The model predictions are represented as their probability density functions. The log normal distribution with mean 125 kN/m^3 and variance 625 kN/m^3 from which the experimental observations (5 points) were sampled represents the real in-situ undrained shear strength of the soil. The mean and standard deviation of the model predictions are tabulated in table 4.7 and figures 4.15 & 4.16. Figure 4.15 shows the conservative nature of model predictions on the mobilized shear strength of the soil when sampled from the posterior, owning to the multiplicative effect of factor of safety which is regarded as a random variable in this case. The results showed reduction in the standard deviation of the model predictions when sampled from the posterior. The mean of the posterior model predictions is much closer to the mean of the real in-situ undrained shear strength of the soil.

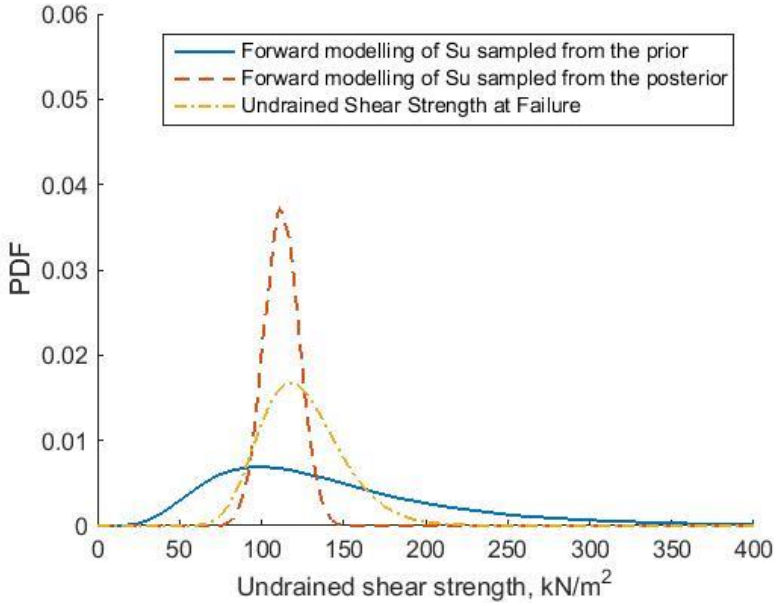

Fig. 4.15. Comparison of model predictions between the experimental data, forward modelling from prior distributions and forward modelling from posterior distributions for Case III.

Estimates	Prior		Posterior	
	Mean	Std	Mean	Std
Model Prediction of mobilized Shear Strength (kN/m^2)	145.622	77.852	112.357	10.85

Table 4.7. Comparison of first order statistics for Case III.

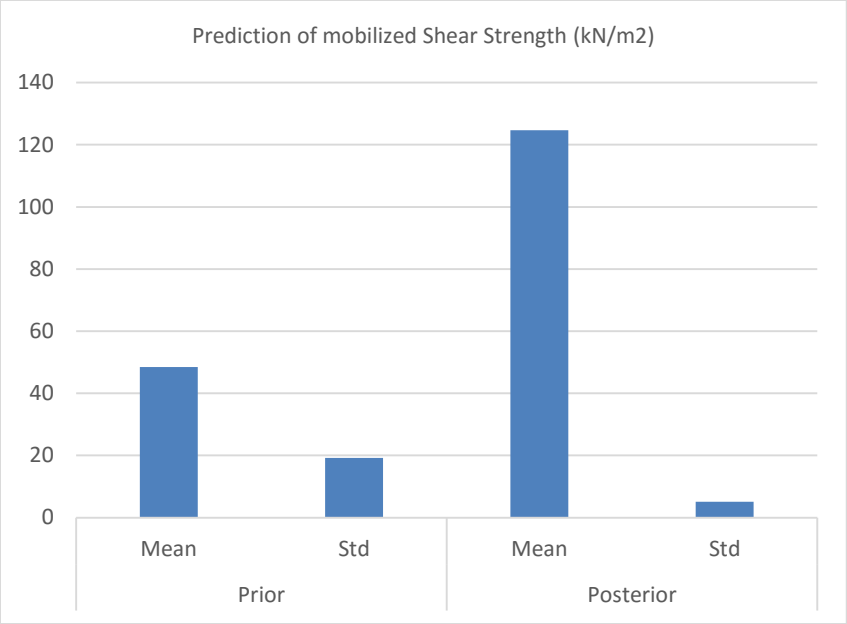

Fig. 4.16. Bar chart of the first order statistics for Case III.

A significant reduction in the estimate of probability of failure is observed with greater certainty on the model predictions as shown in table 4.8. Figure 4.16 shows the first order statistics for Case III.

Estimate	Prior	Posterior
Probability of Failure (%)	52.119	35.488

Table 4.8. Estimates of probability of failure for Case III.

The Bayesian inference for the calibration of the infinite slope model indicated a correlation structure among the model parameters which were initially assumed to be

uncorrelated. Figure 4.17 shows the joint probability histograms between the model parameters. Table 4.9 presents the values of the correlation coefficients between the model parameters.

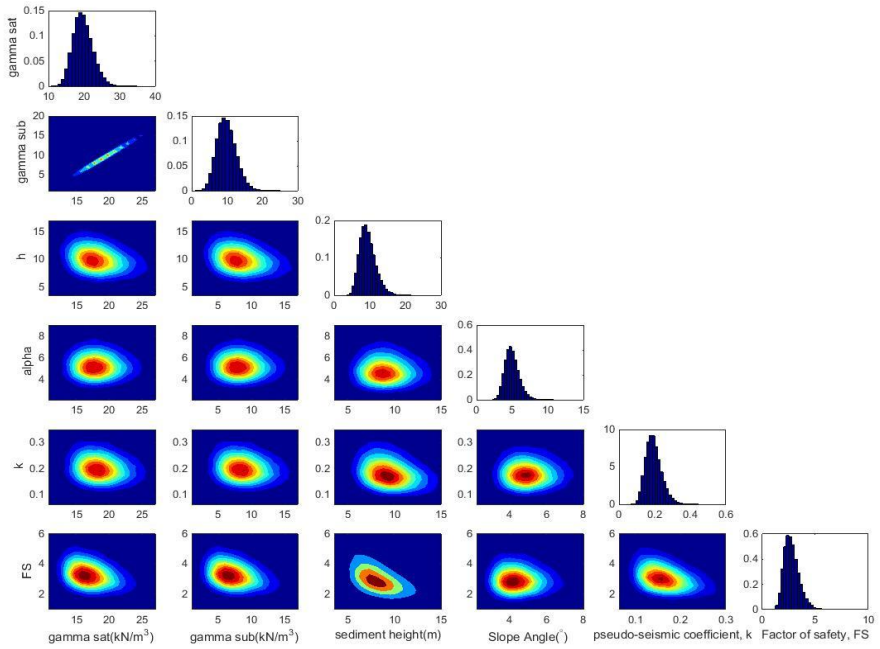

Fig. 4.17. Joint probability histograms of the model parameters for Case III.

Model Parameters	Sat Unit Weight	Sub Unit Weight	Depth	Slope Angle	Seismic Coeff.	Factor of Safety
Sat Unit Weight	1.0000	1.0000	-0.2321	-0.0344	-0.2833	-0.1434
Sub Unit Weight	1.0000	1.0000	-0.2321	-0.0344	-0.2833	-0.1434
Depth	-0.2321	-0.2321	1.0000	-0.0351	-0.4988	-0.2700
Slope Angle	-0.0344	-0.0344	-0.0351	1.0000	-0.0543	-0.0160
Seismic Coeff.	-0.2833	-0.2833	-0.4988	-0.0543	1.0000	-0.3353
Factor of Safety	-0.1434	-0.1434	-0.2700	-0.0160	-0.3353	1.0000

Table 4.9. Correlation coefficients between the model parameters for Case III.

The results presented above were for the case where the prior distribution of the slope angle was centered about 5° with a variance of 1°. Similar analysis were conducted for various angles and the summary of change in the posterior distributions of each model parameter with varying slope angle are presented in figure 4.18.

a)

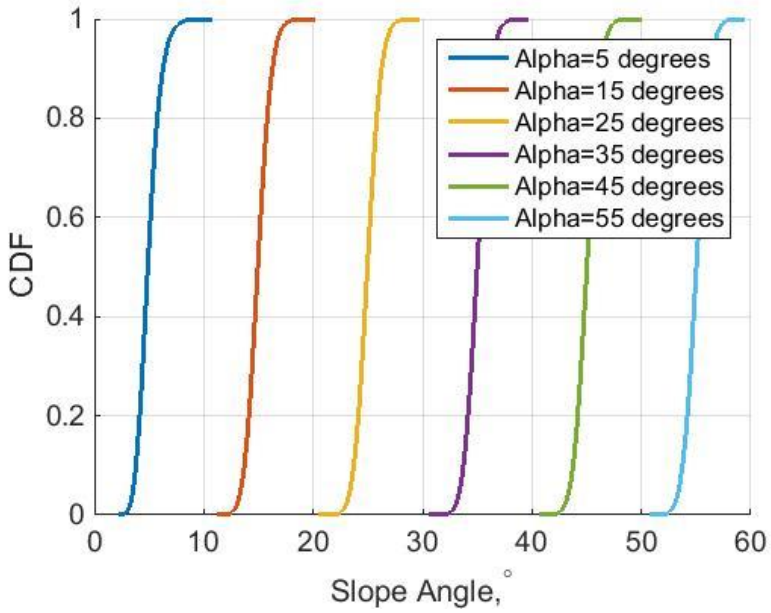

Fig. 4.18. Empirical CDFs of posterior distribution with varying slope angles for Case III. (a) Slope angle. (b) Saturated unit weight. (c) Depth of failure plane. (d) Pseudo static seismic coefficient. (e) Factor of Safety.

b)

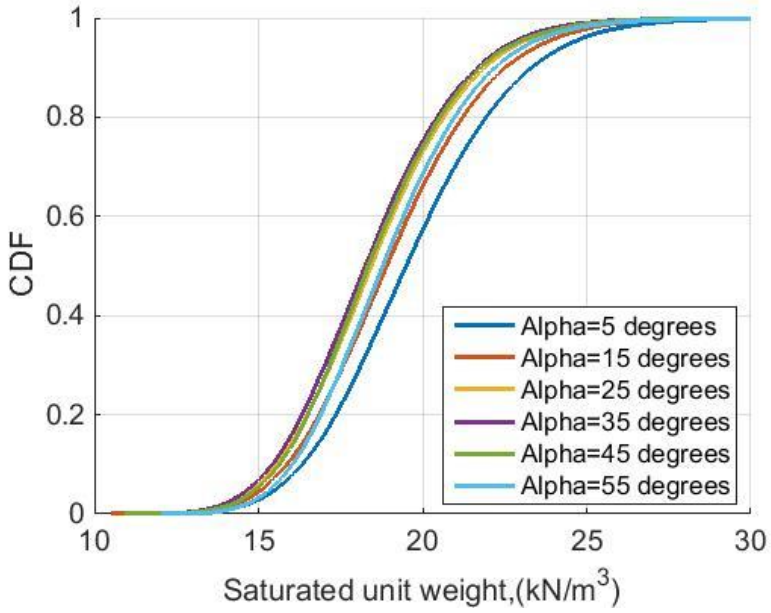

c)

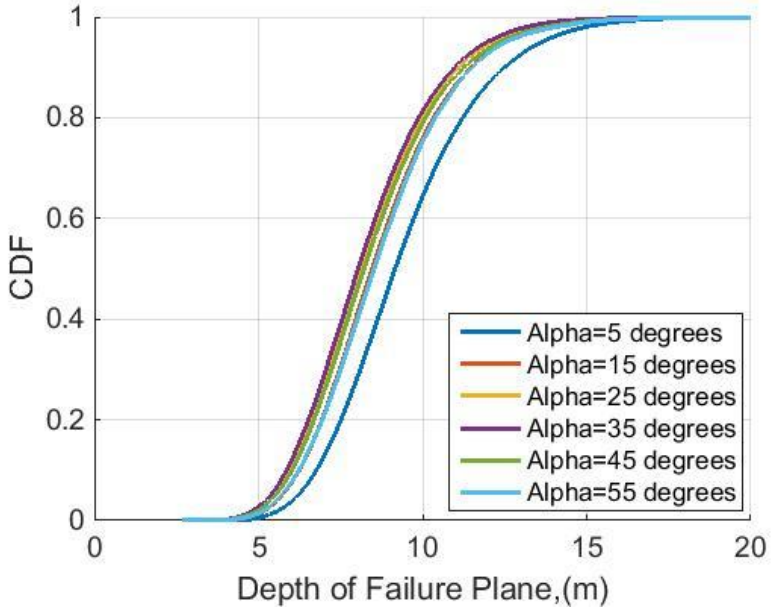

Fig. 4.18. Continued.

d)

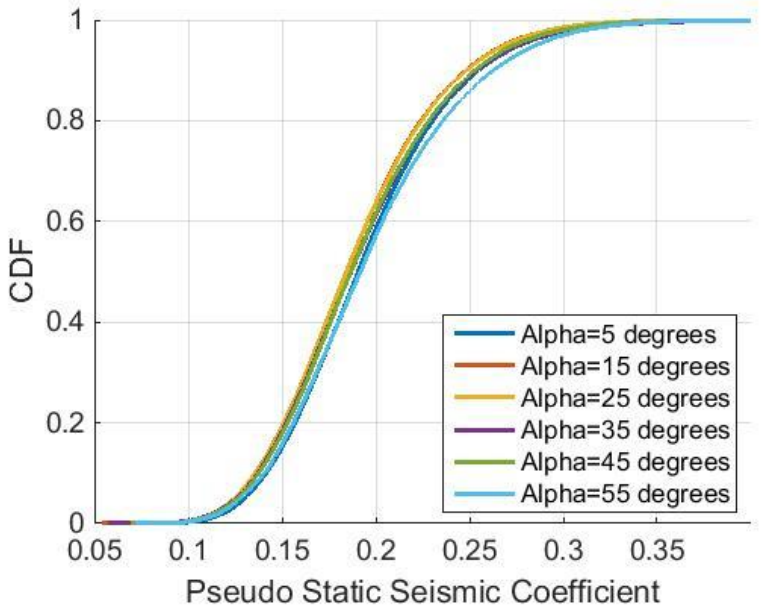

e)

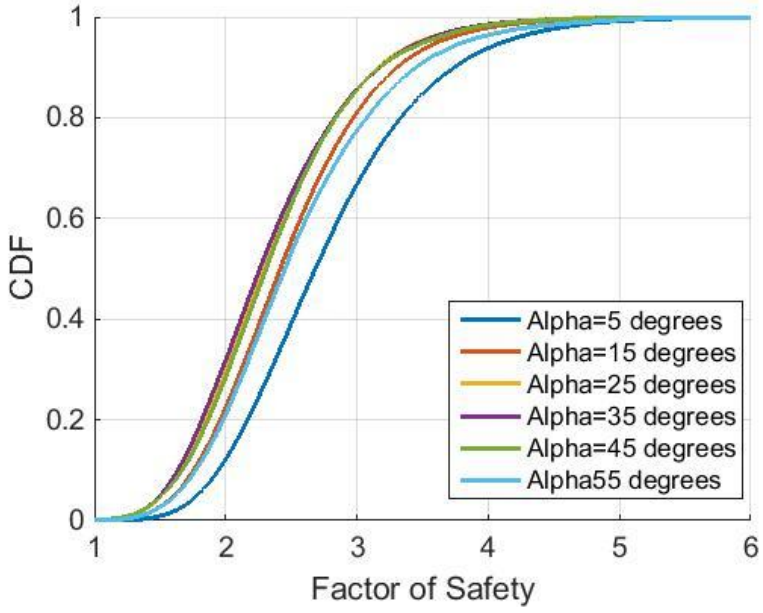

Fig. 4.18. Continued.

4.4. Case IV: Factor of Safety Equals Random Variable, 20 Experimental Observations

Similar to Case III, the factor of safety was considered as a random variable and 20 experimental observations were synthetically generated and used for the calibration of the infinite slope model using the Bayesian inference. The factor of safety was incorporated into the infinite slope model as measure of caution with the model predictions owning to its simplicity. The mobilized shear strength predictions with factor of safety as a random variable were more conservative when compared to the model predictions with factor of safety equaled unity

The figure 4.19 shows the sequence of 600000 samples generated from the posterior distributions of the model parameters and their respective cumulative mean and standard deviation using the MCMC-Metropolis algorithm. The cumulative mean and standard deviation converged after 200000 iterations, therefore the burn in point was chosen to be at 200000. The sequence of samples from 200001 to 600000 for each parameter were used to run the forward simulations of the infinite slope model to estimate the mean and the variance of the model predictions.

a)

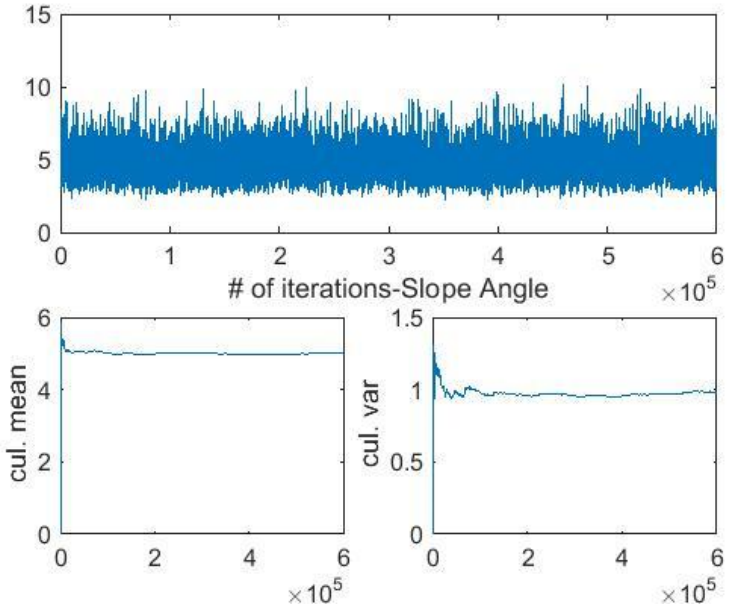

b)

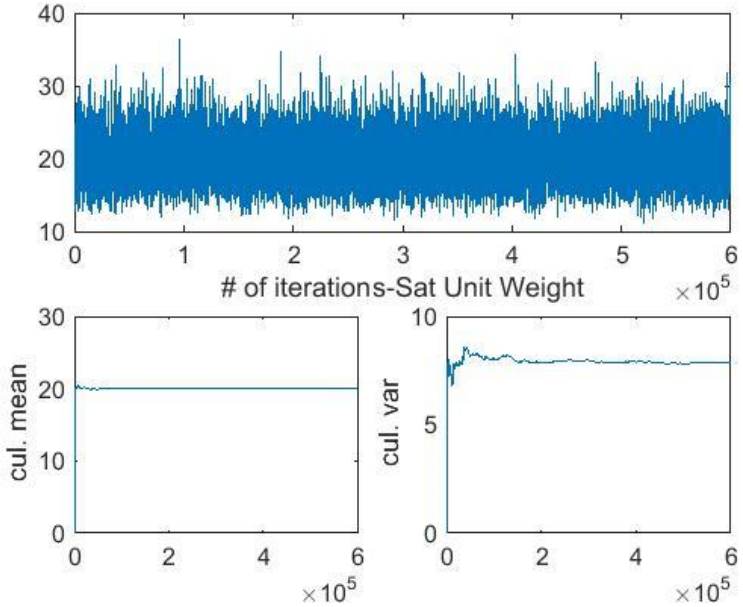

Fig. 4.19. Convergence plots of model parameters for Case IV. (a) Slope angle. (b) Saturated unit weight. (c) Submerged unit weight. (d) Depth of failure plane. (e) Pseudo static seismic coefficient. (f) Factor of Safety.

c)

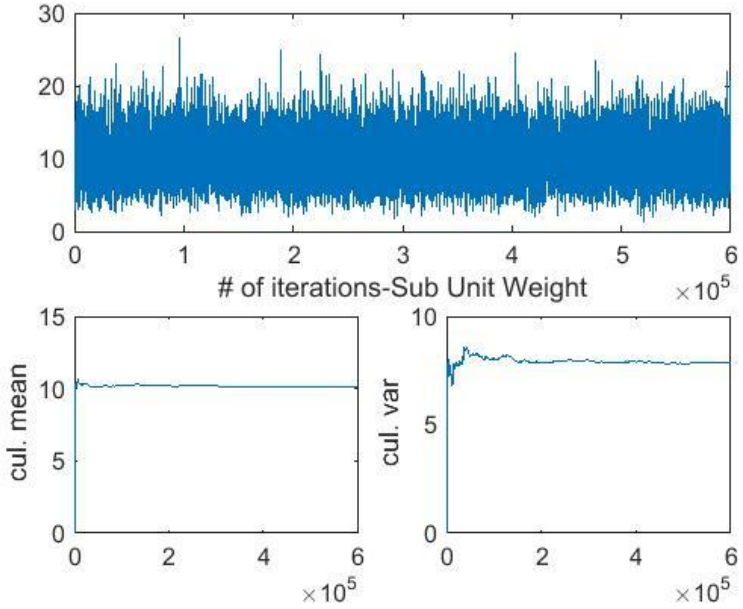

d)

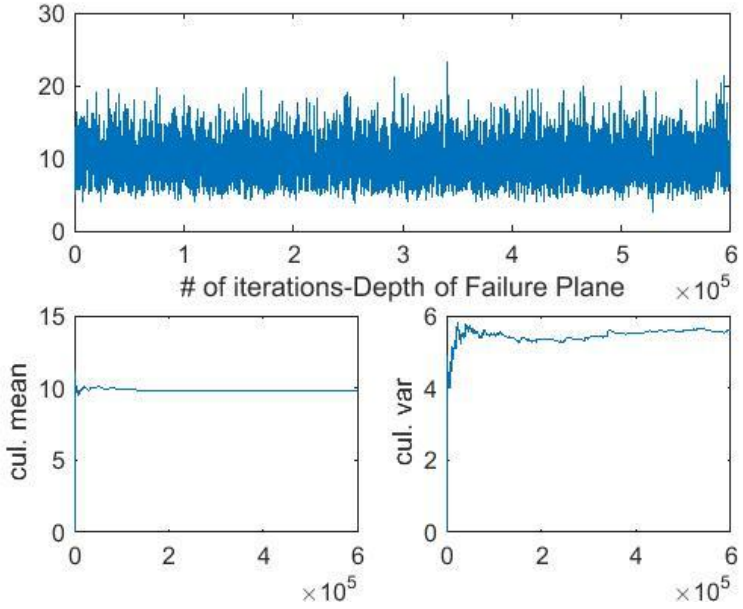

Fig. 4.19. Continued.

e)

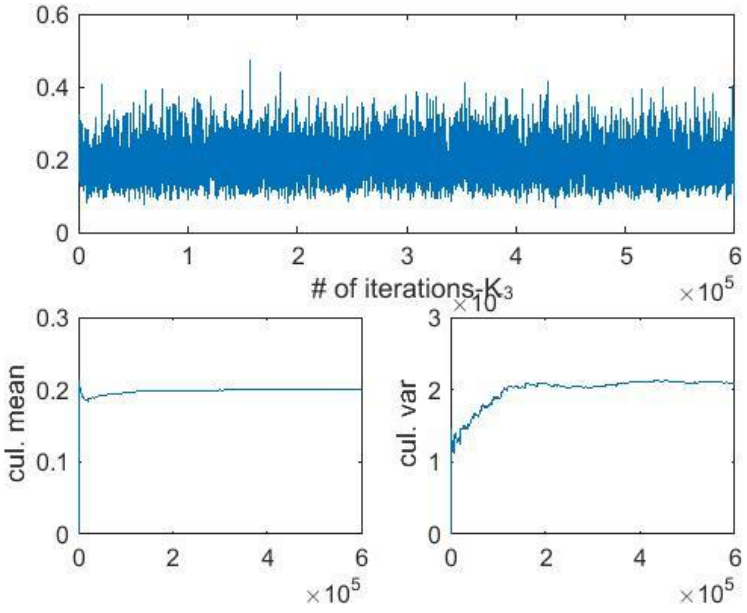

f)

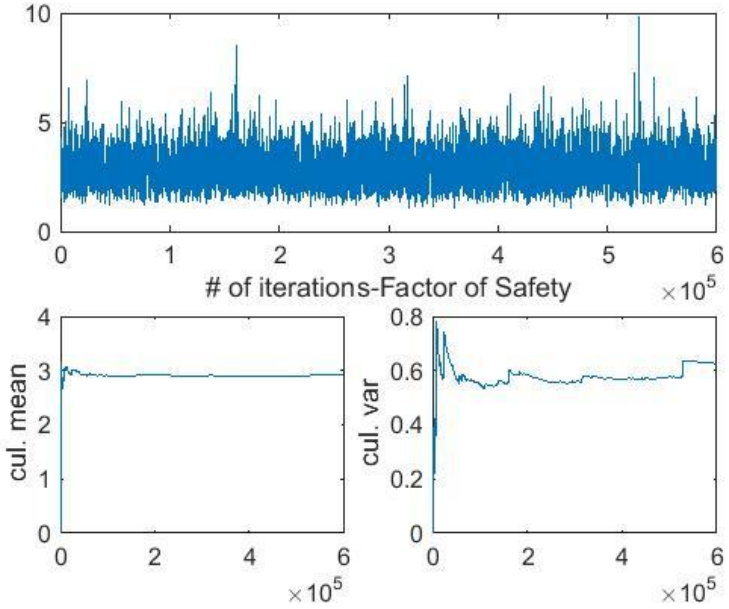

Fig. 4.19. Continued.

The Bayesian inference updated the initial state of evidence (prior distributions) about the model parameters after the calibration of the infinite slope model with 20 experimental observations. The change in the distributions of each model parameters is shown in figure 4.20 as a comparison between their prior and posterior empirical cumulative distribution functions. The sequence of samples after the burn in point of 200000 were used to generate the empirical cumulative distribution function for the posterior distribution for each model parameters. Similar to Case III very slight changes in the distributions of model parameters were observed. However, there were noticeable changes on the distributions of Depth of Failure plane and the Factor of safety.

a)

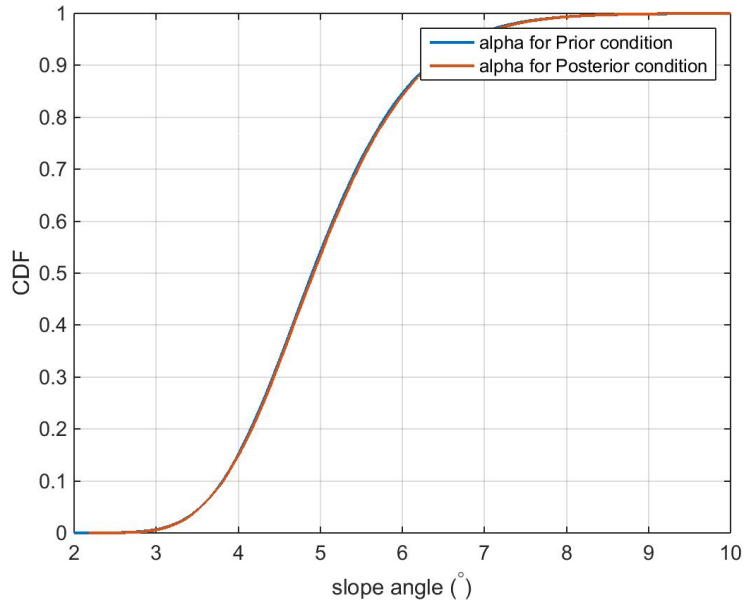

Fig. 4.20. Empirical CDFs of posterior vs prior distributions of the model parameters for Case IV. (a) Slope angle. (b) Saturated unit weight. (c) Submerged unit weight. (d) Depth of failure plane. (e) Pseudo static seismic coefficient. (f) Factor of Safety.

b)

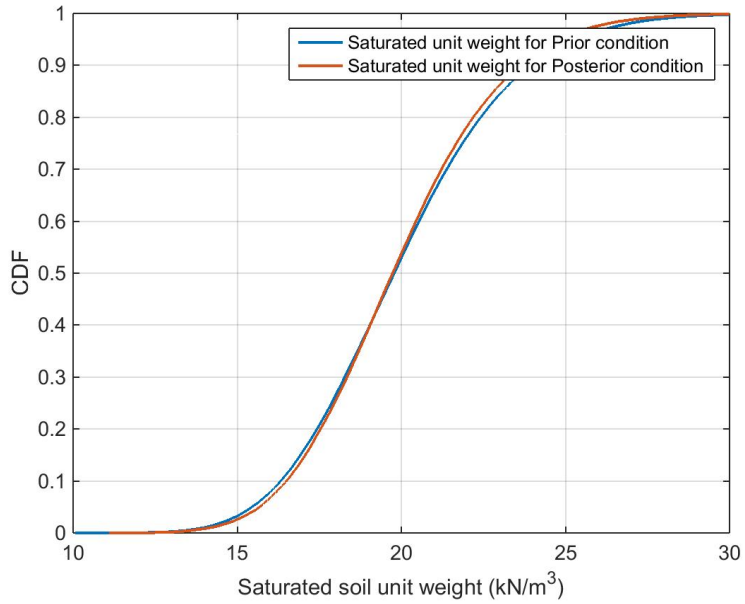

c)

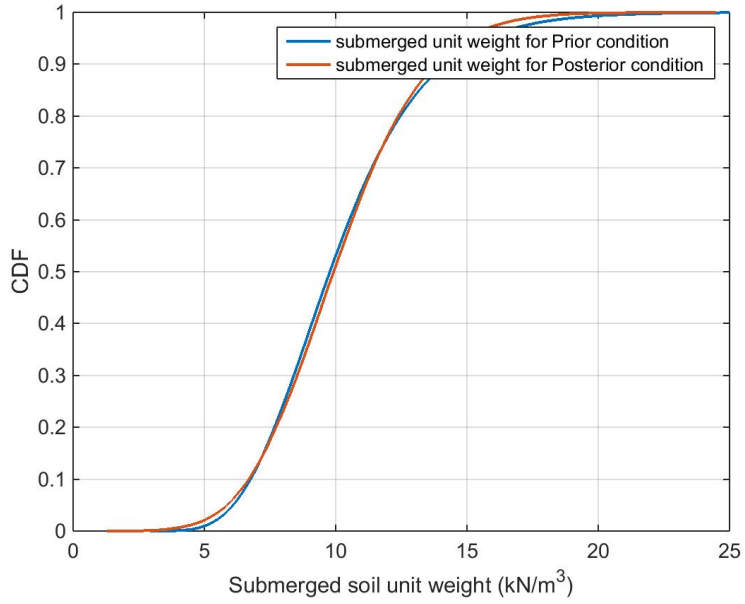

Fig. 4.20. Continued.

d)

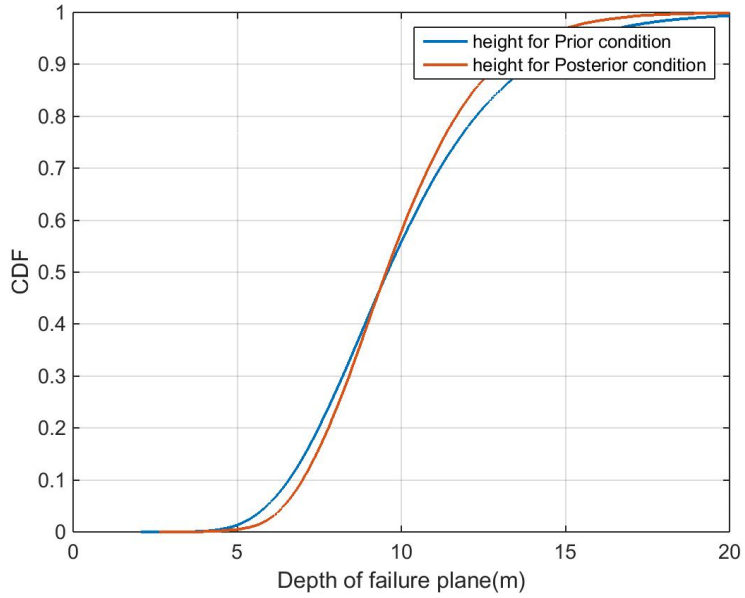

e)

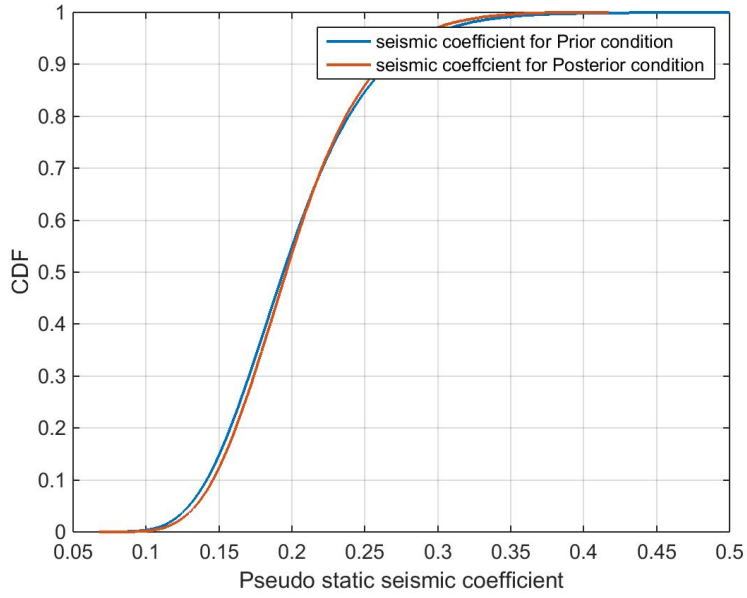

Fig. 4.20. Continued.

f)

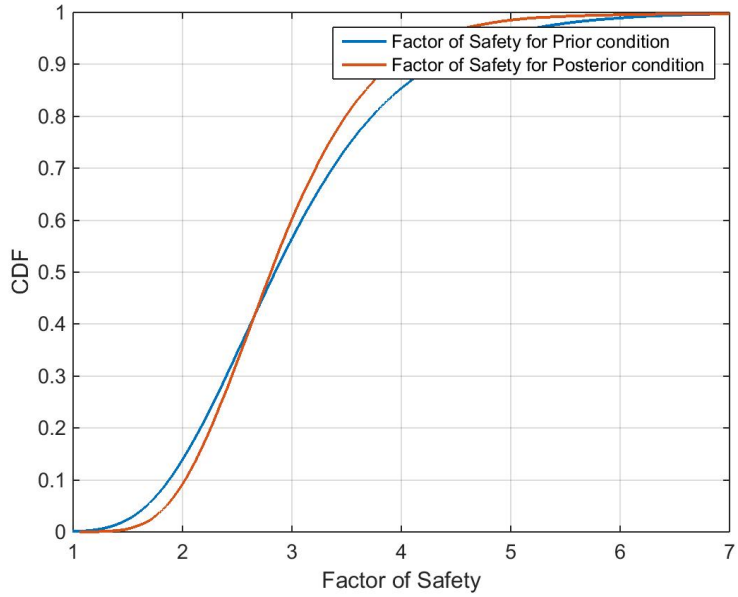

Fig. 4.20. Continued.

The model predictions on the undrained shear strength sampled from the prior distributions and posterior distributions of the model parameters are compared with real data on the undrained shear strength of the soil. The model predictions are represented as their probability density functions. The log normal distribution with mean 125 kN/m^3 and variance 625 kN/m^3 from which the experimental observations (20 points) were sampled represents the real in-situ undrained shear strength of the soil. Similar to Case III, figure 4.21 shows the conservative nature of model predictions on the mobilized shear strength of the soil when sampled from the posterior, owning to the multiplicative effect of factor of safety which is regarded as a random variable in this case. Compared to the previous case (calibration with 5 experimental observations) the results showed a

greater reduction in the standard deviation of the model predictions when sampled from the posterior. The mean of the posterior model predictions nearly captures the mean of the real in-situ undrained shear strength of the soil. Incorporating greater amount of experimental observations (5 points to 20 points) greatly increased the certainty and accuracy of the model predictions. The mean and standard deviation of the model predictions are tabulated in table 4.10 and figures 4.21 & 4.22.

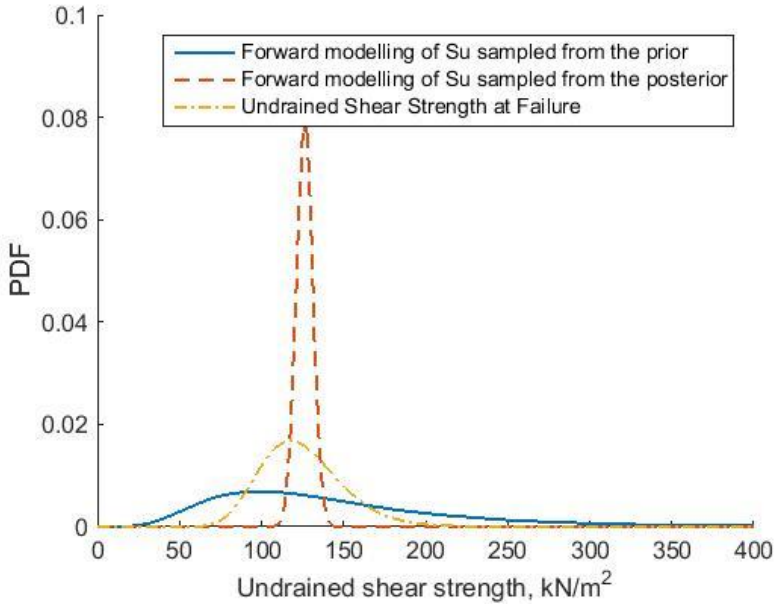

Fig. 4.21. Comparison of model predictions between the experimental data, forward modelling from prior distributions and forward modelling from posterior distributions for Case IV.

Estimates	Prior		Posterior	
	Mean	Std	Mean	Std
Prediction of mobilized Shear Strength (kN/m2)	145.622	77.852	126.159	5.105

Table 4.10. Comparison of first order statistics for Case IV.

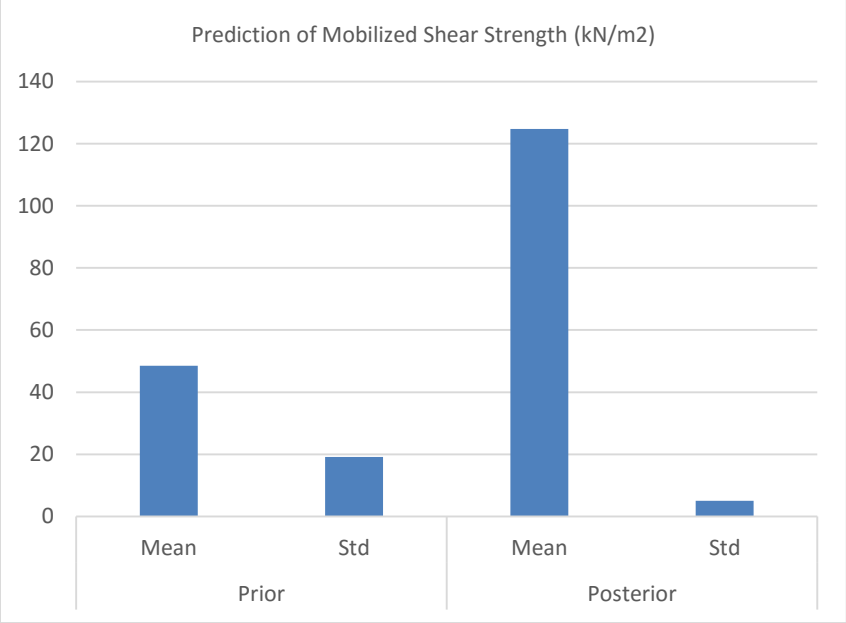

Fig 4.22. Bar chart of the first order statistics for Case IV.

A small decrease in the estimate of probability of failure is observed as shown in table 4.11. Figure 4.22 shows the first order statistics for Case IV.

Estimate	Prior	Posterior
Probability of Failure (%)	52.119	51.283

Table 4.11. Estimates of probability of failure for Case IV.

The Bayesian inference for the calibration of the infinite slope model indicated a correlation structure among the model parameters which were initially assumed to be uncorrelated. Figure 4.23 shows the joint probability histograms between the model parameters. Table 4.12 presents the values of the correlation coefficients between the model parameters.

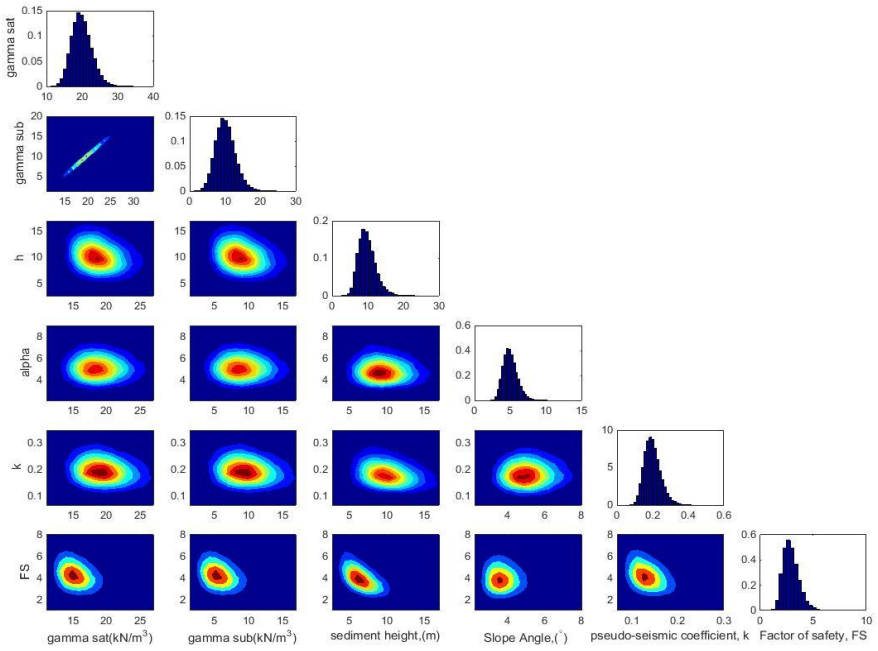

Fig. 4.23. Joint probability histograms of the model parameters for Case IV.

Model Parameters	Sat Unit Weight	Sub Unit Weight	Depth	Slope Angle	Seismic Coeff.	Factor of Safety
Sat Unit Weight	1.0000	1.0000	-0.2392	-0.0325	-0.2938	-0.1447
Sub Unit Weight	1.0000	1.0000	-0.2392	-0.0325	-0.2938	-0.1447
Depth	-0.2392	-0.2392	1.0000	-0.0585	-0.5282	-0.2614
Slope Angle	-0.0325	-0.0325	-0.0585	1.0000	-0.0562	0.0002
Seismic Coeff.	-0.2938	-0.2938	-0.5282	-0.0562	1.0000	-0.3460
Factor of Safety	-0.1447	-0.1447	-0.2614	0.0002	-0.3460	1.0000

Table 4.12. Correlation coefficient between the model parameters for Case IV.

The results presented above were for the case where the prior distribution of the slope angle was centered about 5° with a variance of 1°. Similar analysis were conducted

for various angles and the summary of change in the posterior distributions of each model parameter with varying slope angle are presented in figure 4.24.

a)

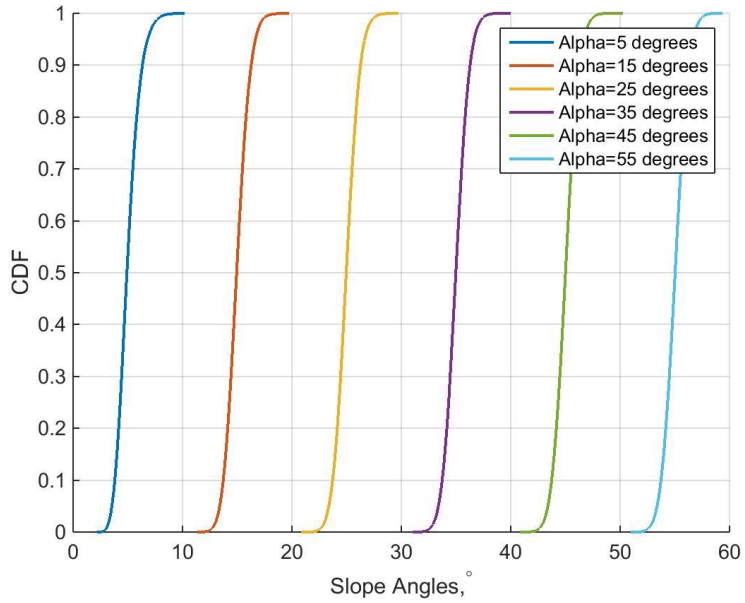

Fig. 4.24. Empirical CDFs of posterior distribution with varying slope angles for Case IV. (a) Slope angle. (b) Saturated unit weight. (c) Depth of failure plane. (d) Pseudo static seismic coefficient. (e) Factor of Safety.

b)

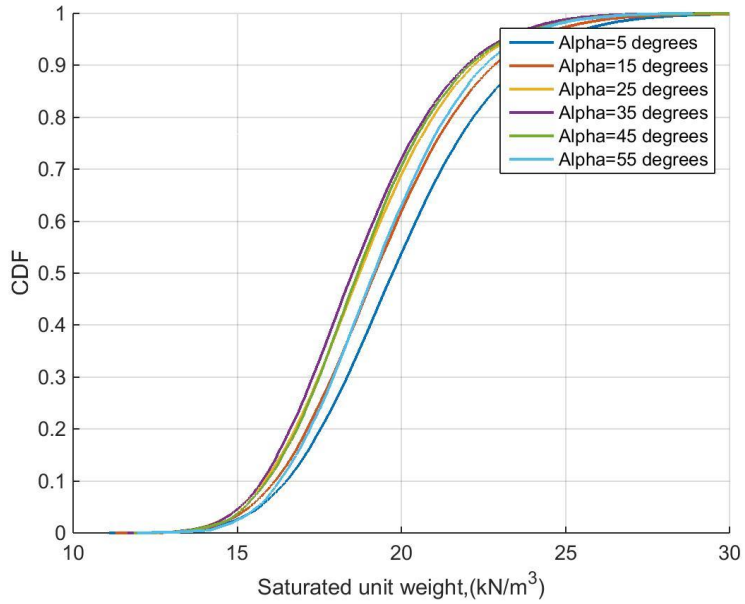

c)

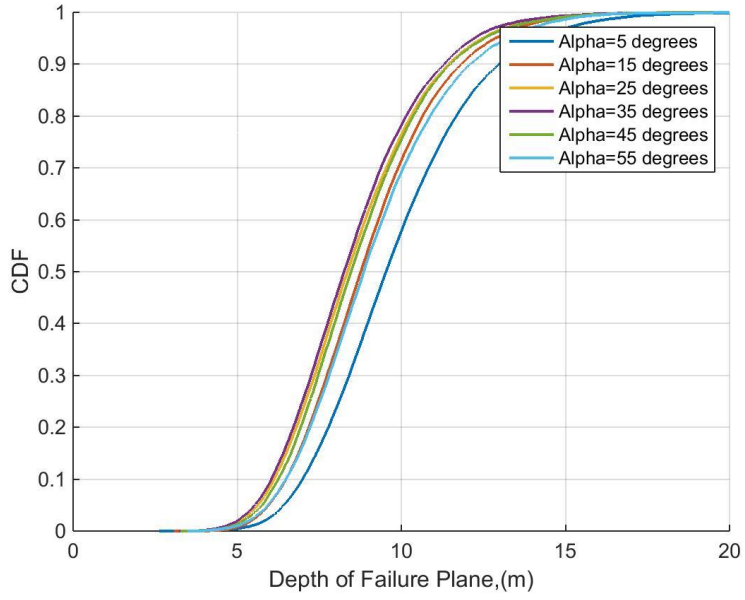

Fig. 4.24. Continued.

d)

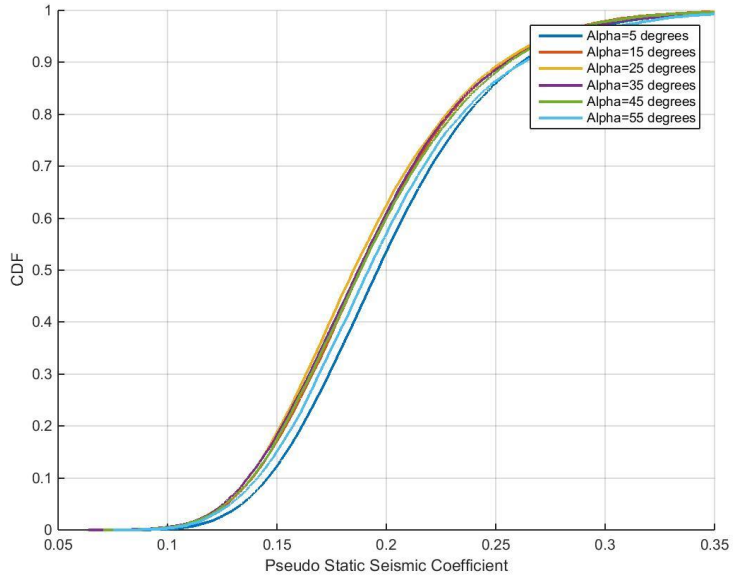

e)

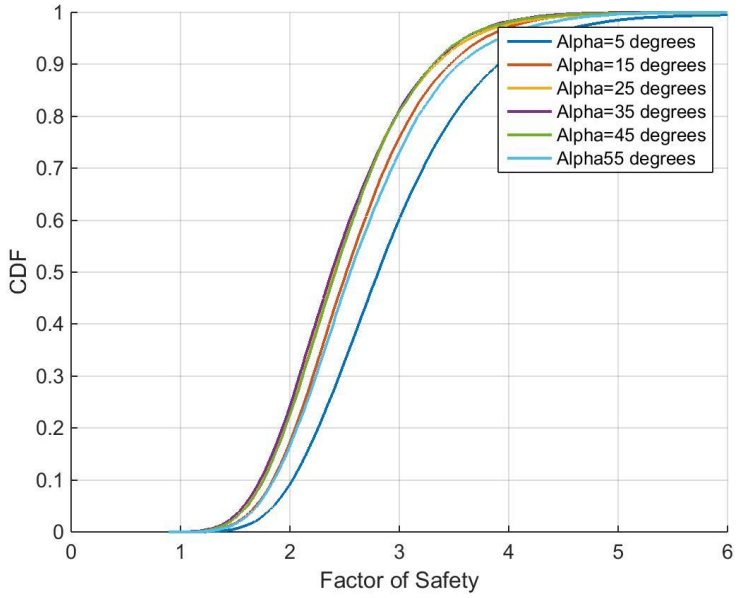

Fig. 4.24. Continued.

4.5. Analysis

The MCMC- Metropolis algorithm was used to sample from the posterior distribution of the model parameters. 600000 iterations were run to attain convergence of the cumulative mean and cumulative standard deviation of the model parameters for each case as illustrated in figures 4.1, 4.7, 4.13 and 4.19. The burn in point was set visually at 200000 iterations. All the samples from 200001 to 600000 represented the steady state posterior distributions of the model parameters and were used to run the forward model to attain the posterior model predictions on the mobilized shear strength of the soil. Comparison of model predictions sampled from posterior distributions of the model parameters with Monte-Carlo forward model simulations based on the prior distributions show a significant reduction uncertainty (standard deviation) in all the four cases.

The Log-Normal distribution from which the experimental observations were sampled had a mean of 125 kN/m^3 and standard deviation of 25 kN/m^3 which represented real in-situ undrained shear strength of the soil. The objective for the calibration of the infinite slope model with the experimental observation assuming limit state was to achieve more certain and accurate model predictions closer to the mean of the real data. The reduction in standard deviation for cases I to IV shows greater certainty in model predictions after the probabilistic calibration of the infinite slope model with the experimental observations. In case I the mobilized undrained shear strength sampled from the posterior distribution has a reduced standard deviation of 19.24 and mean 105.1 closer to the real data as represented in figures 4.3 & 4.4 and table

4.1. Case II tests the influence of greater amount of data on the model predictions. Calibration of the infinite slope forward model with 20 data points on undrained shear strength as compared to 5 points in Case II show a greater level of certainty on the model predictions. Moreover, the mean of the model predictions nearly equals the mean of the real process (mean of the experimental data) as illustrated in figures 4.9 & 4.10 and table 4.4. This shows probabilistic calibration with larger amount of data points has a positive influence on reducing the uncertainty associated with the model predictions. In Cases III & IV, the factor of safety is incorporated in the infinite slope model as a random variable. The uncertainty associated with the model predictions is reduced when sampled from the posterior distribution as illustrated in figures 4.15 & 4.16 and table 4.7 for Case III and figures 4.21 & 4.22 and table 4.10 for Case IV. Moreover, the reduction in uncertainty become more pronounced when the probabilistic calibration is done with 20 data points in Case IV. Therefore, the trends discovered in Cases I & II are consistent with Cases III & IV. Figure 4.25 and table 4.13 illustrate the comparison of the model predictions sampled from the posterior distribution s of the model parameters and the Monte-Carlo forward simulation on the basis of the prior distributions with the experimental data for all the four cases.

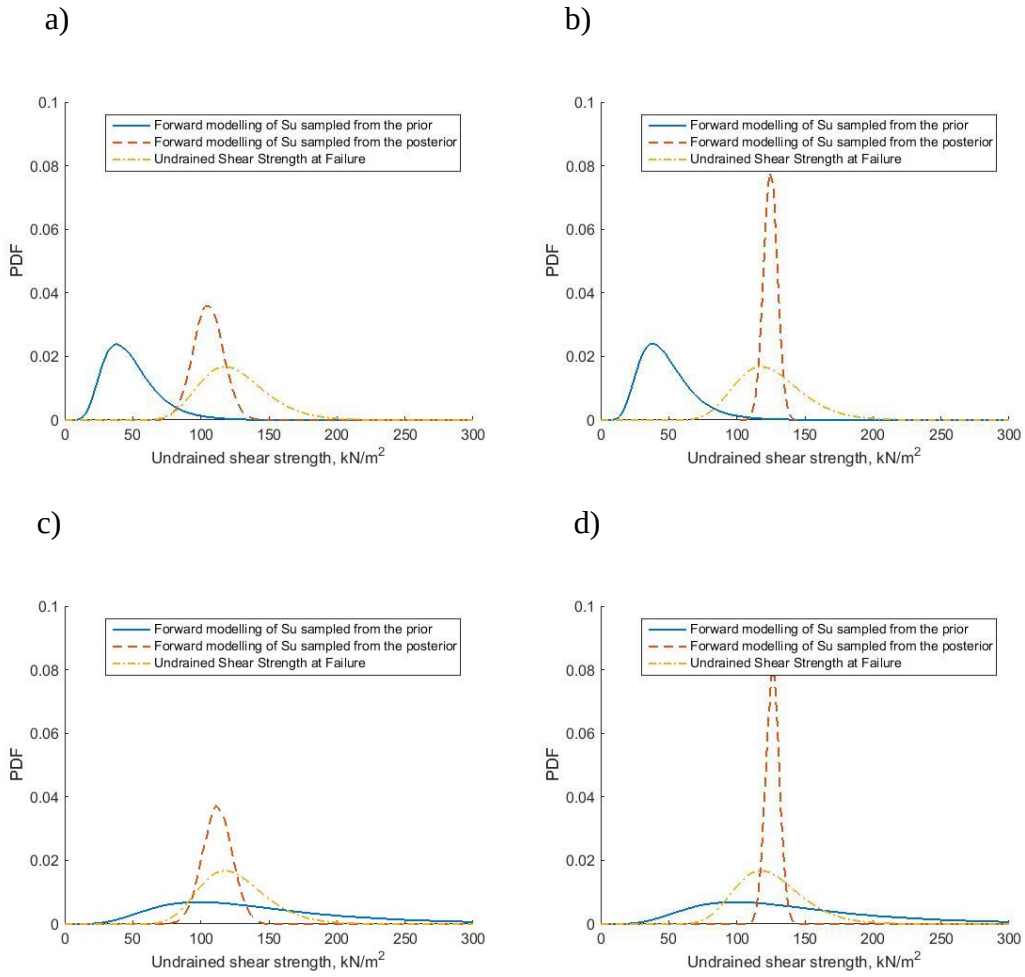

Fig. 4.25. Comparison of model predictions for Cases I to IV. (a) Cases I. (b) Case II. (c) Case III. (d) Case IV.

Case	Prior		Posterior	
	Mean (kN/m^2)	Std (kN/m^2)	Mean (kN/m^2)	Std (kN/m^2)
I Limit State (5 points)	49	19.24	105.01	11.03
II Limit State (20 points)	49	19.24	124.69	5.08
III Factor of Safety=Random Variable (5 points)	145.62	77.85	112.36	10.85
IV Factor of Safety=Random Variable (20 points)	145.62	77.85	126.16	5.11

Table 4.13. Comparison of first order statistics for Cases I to IV.

A major advantage of Bayesian inference was the indication of the correlation structure among the model parameters and their changes with varying degree of evidence on the parameters, experimental data and model complexity. The model parameters were initially considered uncorrelated. Figures 4.5, 4.11, 4.17 and 4.23 illustrated the correlation structure between the model parameters for Cases I to IV respectively through the joint probability histogram taking two parameters at a time. The figures showed a negative correlation between some of the model parameters in all the four cases. Figure 4.5 illustrates the correlation structure among the model parameters in Cases I, which showed a negative correlation between the depth of the failure plane and the saturated unit weight of the soil. A negative correlation was also indicated between the saturated unit weight and the pseudo static seismic coefficient. The depth of failure plane and the pseudo static seismic coefficient were negatively correlated with a high correlation coefficient of about -0.575. Similar trends were observed with Case II as illustrated in figure 4.11. Higher amount of experimental observations used in the model calibration resulted in more distinct correlation structure.

Figures 4.17 and 4.23 illustrated the correlation structure between the model parameters in Cases III and IV. A negative correlation between the factor of safety and the each of the other parameters were noticed.

Probability of failure is defined as the probability of the safety margin lesser than unity. Cases I and II provided lower estimates of the probabilities of failure when sampled from the prior distributions of the model parameters. This was due to the predictions of non-conservative values of the mobilized shear strength. Estimates of the

probabilities of failure for cases I and II increased after calibration with 5 and 20 experimental observations respectively moving towards the true probability of failure. Cases III and IV, however provided higher estimates of the probability of failure when sampled from the prior distributions of the model parameters due to the multiplicative effect of the factor of safety which predicted conservative values of the mobilized shear strength. Model calibration with 5 and 20 experimental observations reduce the estimate of the probability of failure towards the actual probability of failure. Quantitative slope stability assessment in previous works as reviewed earlier using probabilistic methods Monte-Carlo methods, FOSM or FORM did not study the influence of more certain model predictions on the probability of failure or the reliability index. Use of the Bayesian paradigm for probabilistic model calibration and probability of failure estimation proposed here shows the influence of more certain and accurate model predictions on probability of failure estimations.

5. CONCLUSIONS

The Bayesian paradigm incorporates the experimental data (on the in-situ undrained shear strength of the soil), infinite slope model and initial state of evidence on the model parameters to achieve more certain and accurate model predictions. Greater certainty and accuracy of model predictions reduce the value of probability of failure and increase reliability. This thesis uses the Bayesian framework to estimate the probability of failure using the infinite slope model for varying slope angles. More complex slope stability models can be used to determine the risk of landslides. The Bayesian inference indicates the correlation structure among the model parameters which were initially considered uncorrelated. This allows to estimating the sampling scenarios and their corresponding confidence gains before a field investigation is conducted.

REFERENCES

Arson, C., & Medina-Cetina, Z. (2015). Bayesian paradigm to assess rock compression damage models. *Environmental Geotechnics*, 2, 155-165.

Bruschi, R., Bughi, S., Spinazzè, M., Torselletti, E., & Vitali, L. (2006). Impact of debris flows and turbidity currents on seafloor structures. *Norwegian Journal of Geology*, 86, 317-337.

Chowdhury, R., & Flentje, P. (2003). Role of slope reliability analysis in landslide risk management. *Bulletin of Engineering Geology and the Environment*, 62, 41-46.

Prior, D.B., & Coleman M. James. (1978). Disintegrating retrogressive landslides on very-low angle subaqueous slopes, Mississippi delta. *Marine Geotechnology*, 3, 37-60.

El-Ramly, H., Morgenstern, N.R., & Cruden, D.M. (2002). Probabilistic slope stability analysis for practice. *Canadian Geotechnical Journal*, 39, 665-683.

Fredlund, D.G., Krahn, J., & Pufahl, D.E. (1981). The relationship between limit equilibrium slope stability methods. *Proceedings of the International Conference on Soil Mechanics and Foundations.* Stockholm, Sweden, 3, 409-416.

Gauer, P., Medina-Cetina, Z., Lied, K., & Kristensen, K. (2009). Optimization and probabilistic calibration of avalanche block models. *Cold Regions Science and Technology*. 59, 251-258.

Gilbert, R.B., Lacasse, S., & Nadim, F. (2014). Advances in geotechnical risk and reliability for offshore applications. In L. Zhang, Y. Wang, G. Wang, & L. Dianqing (Eds.), *Geotechnical Safety And Risk IV* (pp 29-42). Hong Kong: CRC Press.

Gordon, A. F., & Vanmarcke, E. H. (1990). Simulation of random fields via local average subdivisions. *Journal of Engineering Mechanics*. 116, 1733-1749.

Griffiths, D.V. & Fenton, G.A. (2004). Probabilistic slope stability analysis by finite elements. *Journal of Geotechnical and Geoenvironmental Engineering*, 130, 1367-1378. 507-518.

Griffiths, D.V., Huang, J. & Fenton, G.A. (2009). Influence of spatial variability of slope reliability using 2-D random fields. *Journal of Geotechnical and Geoenvironmental Engineering*, 135, 1367-1378.

Griffiths, D.V., Huang, J. & Fenton, G.A. (2011). Probabilistic infinite slope analysis. *Computers and Geotechnics*, 4, 577-584.

Haneberg, W. C. (2004). A rational probabilistic method for spatially distributed landslide hazard assessment. *Environmental & Engineering Geoscience*, 1, 27-43.

Haneberg, W. C. (2012). Spatially distributed probabilistic assessment of submarine slope stability offshore site investigation and geotechnics. Proc., *7th International Offshore Site Investigation and Geotechnics Conference.* London, U.K., 551-556.

Haneberg, W. C., Bruce, B., & Drazba, M.C. (2013). Using qualitative slope hazard maps and quantitative probabilistic slope stability models to constrain least-cost pipeline route optimization. Paper was presented at the *Offshore Technology Conference.* Houston, Texas, USA.

King, T., Phillips R., & Johansen, C. (2011). Pipeline routing and burial depth analysis using GIS software. Paper presented at the *OTC Arctic Technology Conference.* Houston, Texas, USA.

Lacasse, S., & Nadim, F. (2007). Probabilistic geotechnical analyses for offshore facilities. *Georisk*, 1, 21-42.

Locat, J., & Lee, H. J. (2000). Submarine landslides: Advances and challenges. Proc., *8th International Symposium on Landslides*. Cardiff, U.K.

Medina-Cetina, Z., Kang, J. W., Esmailzadeh, S., & Kallivokas, L. (2013). Bayesian inversion of heterogeneous media: Introducing the next generation of integrated studies for offshore site investigations. Paper presented at *Offshore Technology Conference*. Houston, Texas, USA.

Medina-Cetina, Z., & Cepeda, J. (2010). Probabilistic Classification of local rainfall-thresholds for the landslide triggering. Paper presented at *EGU General Assembly*. Vienna, Austria.

Melo, C., & Sharma, S. (2004). Seismic coefficients for pseudostatic slope analysis. Paper presented at the *13th World Conference on Earthquake Engineering*, Vancouver, British Columbia, Canada.

Morgenstern, N. R. (1967). Submarine slumping and the initiation of turbidity currents. In A. Richards (Ed.), *Marine Geotechnique* (pp 189-220).

Pinder, D. (2001). Offshore oil and gas: Global resource knowledge and technological change. *Ocean and Coastal Management*. 44, 570-600

Prior, D. B., & Coleman, M. J. (1978). Disintegrating retrogressive landslides on very low angle subaqueous slopes, Mississippi delta. *Marine Geotechnology*, 3, 37-60.

Ranali, M., Gottardi, G., Medina-Cetina, Z., & Nadim, F. (2010). Uncertainty quantification in the calibration of a dynamic viscoplastic model of slow slope movements. *Landslides*, 7, 31-41.

Randolph M. F., & White, D. J. (2012). Interaction forces between pipelines and submarine slides-A geotechnical viewpoint. *Ocean Engineering*, 48, 32-37.

Remendo, J., Bonachea, J., & Cendrero, A. (2008). Quantitative landslide risk assessment and mapping on the basis of recent occurrences. *Geomorphology*, 94, 496-507.

Ochoa. R., Nadim, F., Cepeda, M.A., & Liu, Z. (2015). Hazard analysis of seismic submarine slope instability. *Georisk: Assessment and Management of Risk for Engineered Systems and Geohazards*, 9, 128-147.

Sivakumar, G. L., & Mukesh, M.D. (2003). Risk analysis of landslides- A case study. *Geotechnical and Geological Engineering*, 21, 113-127.

Souza, R.L., Karam, K., & Einstein, H. H. (2014). Exploration analysis for landslide risk management. *Georisk: Assessment and Management of Risk for Engineered Systems and Geohazards*, 8, 155-170.

Wang, J.P., & Huang, D. (2013). Slope failure probability under earthquake condition by Monte-Carlo Simulation: Methodology and Example for an infinite slope. In S. Chakraborty & G. Bhattacharya (Eds.), *Proceedings of the International Symposium*

on Engineering under Uncertainty: Safety Assessment and Management (pp. 643-652). India: Springer.

Wang, Y., Cao, Z., & Au, S.K. (2010). Efficient Monte Carlo simulation of parameter sensitivity in probabilistic slope stability analysis. *Computers and Geotechnics*, 37, 1015-1022.

Zakeri, A., Hoeg, K., & Nadim, F. (2008). Submarine debris flow impact on pipelines-Part 1: Experimental investigation. *Coastal Engineering*, 55, 1209-1218.